ULSAN NATIONAL INSTITUTE OF
SCIENCE AND TECHNOLOGY

Master's Thesis

Research on Differential Power Processing Techniques of Photovoltaic Systems for Effective Power Generation

Seungbin Park

Department of Electrical Engineering

Graduate School of UNIST

2020

ULSAN NATIONAL INSTITUTE OF
SCIENCE AND TECHNOLOGY

Research on Differential Power Processing Techniques of Photovoltaic Systems for Effective Power Generation

Seungbin Park

Department of Electrical Engineering

Graduate School of UNIST

ULSAN NATIONAL INSTITUTE OF
SCIENCE AND TECHNOLOGY

Research on Differential Power Processing Techniques of Photovoltaic Systems for Effective Power Generation

A thesis
submitted to the Graduate School of UNIST
in partial fulfillment of the
requirements for the degree of
Master of Science

Seungbin Park

12 Dec. 2019
Approved by
Advisor
Jee-Hoon Jung

ULSAN NATIONAL INSTITUTE OF
SCIENCE AND TECHNOLOGY

Research on Differential Power Processing Techniques of Photovoltaic Systems for Effective Power Generation

Seungbin Park

This certifies that the thesis of Seungbin Park is approved.

12 Dec. 2019

Advisor: Jee-Hoon Jung

Jingook Kim: Thesis Committee Member #1

Jeon, Jeong hwan: Thesis Committee Member #2

ULSAN NATIONAL INSTITUTE OF
SCIENCE AND TECHNOLOGY

Abstract

Due to increasing energy demand, depletion of fossil fuels, and environmental pollution, there are growing interests in the photovoltaic (PV) power generation system, which is environmentally friendly and efficient. However, the mismatch among the series-connected PV modules decreases the DC voltage and output power at the maximum power point (MPP). To solve this problem, the differential power processing (DPP) system which can operate at MPP of each PV module regardless of mismatch in power generations, which is caused by partial shades has been proposed. In the DPP system, DPP converters are connected in parallel to the PV modules, which control each PV module in its own MPP. As a result, it is possible to produce more power compared to a series-connected system in partial shading conditions. In addition, the DPP converter only compensates for power variations between panels, resulting in low power capacity, high cost effectiveness, and low loss due to converter operation. However, the DPP system has various structures, and its design method suitable for each structure should be considered. In addition, when many DPP converters are configured, it makes the DPP system less reliable than simple series-connected PV systems.

In this thesis, the DPP system for the PV power generation is proposed. The design methodology of a bidirectional flyback converter used as the DPP converter for the PV-to-bus DPP structure is also introduced. This thesis also develops a protection algorithm to improve the reliability of the DPP system. It is verified by modeling the DPP system and its failure conditions using a power hardware-in-the-loop (PHIL) simulation technique. Besides, high accurate indoor experimental method used to verify the developed DPP system performance is developed by using a PV emulation method in MPP. The experimental results show the comparison of the output power between the series connection system and the DPP system under various partial shade conditions. As further work, an on/off algorithm suitable for the DPP system employing multiple string diode PV modules is proposed and verified by simulation.

ULSAN NATIONAL INSTITUTE OF
SCIENCE AND TECHNOLOGY

ULSAN NATIONAL INSTITUTE OF SCIENCE AND TECHNOLOGY

Contents

ULSAN NATIONAL INSTITUTE OF SCIENCE AND TECHNOLOGY

List of Figures

ULSAN NATIONAL INSTITUTE OF
SCIENCE AND TECHNOLOGY

ULSAN NATIONAL INSTITUTE OF SCIENCE AND TECHNOLOGY

List of Tables

ULSAN NATIONAL INSTITUTE OF
SCIENCE AND TECHNOLOGY

I. Introduction

Recently, there is a growing interest in renewable energy sources, such as fuel cell, wind turbine, and solar energy. Among them, photovoltaic (PV) power generation is particularly attractive because it enables efficient power generation regardless of location [1]. Traditionally, the PV is connected as a series to step up the output voltage of the PV module easily for transferring to the grid. Fig 1.1 (a) show the PV series connection system structure. The PV series connection system is simple in that PV modules are connected in series or diodes are connected in parallel to PV modules. However, the conventional series connection system shares the same series current in all the panels. It causes each panel cannot operate at the maximum power point (MPP) when the PV modules receives uneven solar irradiance. This problem reduces the power generation and power transfer efficiency [2,3].

As a solution to this problem, a full power processing (FPP) system such as DC optimizer and micro-inverter has been proposed [4]-[7]. Fig 1.1 (b) show the FPP system structure. In the FPP processing system, one FPP converter is connected to parallel per PV module. Therefore, the FPP system doesn't share the same series current. FPP converter performs maximum power point tracking (MPPT) for one each PV modules. Thus, each panel can operate its own MPP and the PV system can obtain more generation power and system efficiency than a conventional series connection system at partial shade conditions. However, the FPP system is required a relatively large power capacity of converter because all power of PV is converted through the FPP converter. It causes large power loss of the converter and costs for converter configuration. The system efficiency of FPP is the same as the efficiency of the FPP power converter.

Another solution to the problem of the series connection system is a differential power processing (DPP) system [8]-[10]. Fig 1.1 (c) shows the DPP system structure. Like the FPP system, the DPP system has one DPP converter which is connected to parallel per PV module. DPP converter can make other paths of the current, so the DPP system doesn't share the same series current. Therefore, each panel can operate its own MPP. As a result, DPP achieves higher efficiency than a conventional series connection system under uneven solar irradiance conditions. The DPP converters only process power deviation of the PV modules to make current path. According to partial shade condition, operation power DPP converters is determined. Therefore, the DPP system has smaller capacity of converter and lower cost for system configuration and power loss of the converter than the FPP system. Also, in the various partial shade condition, the higher DPP system efficiency can be obtained than the FPP system. For this reason, DPP systems have been studied in recent years [11]-[13].

The DPP system has various structures. Therefore, design methodology suitable for each structure should be considered. Fig. 1.2 shows an example of the DPP system structure, referred to as PV-to-Bus structure [14]. In this structure, the DPP converter has an input port connected to the output of the PV module. The output port of the DPP converter is connected to the output of the series PV module.

ULSAN NATIONAL INSTITUTE OF SCIENCE AND TECHNOLOGY

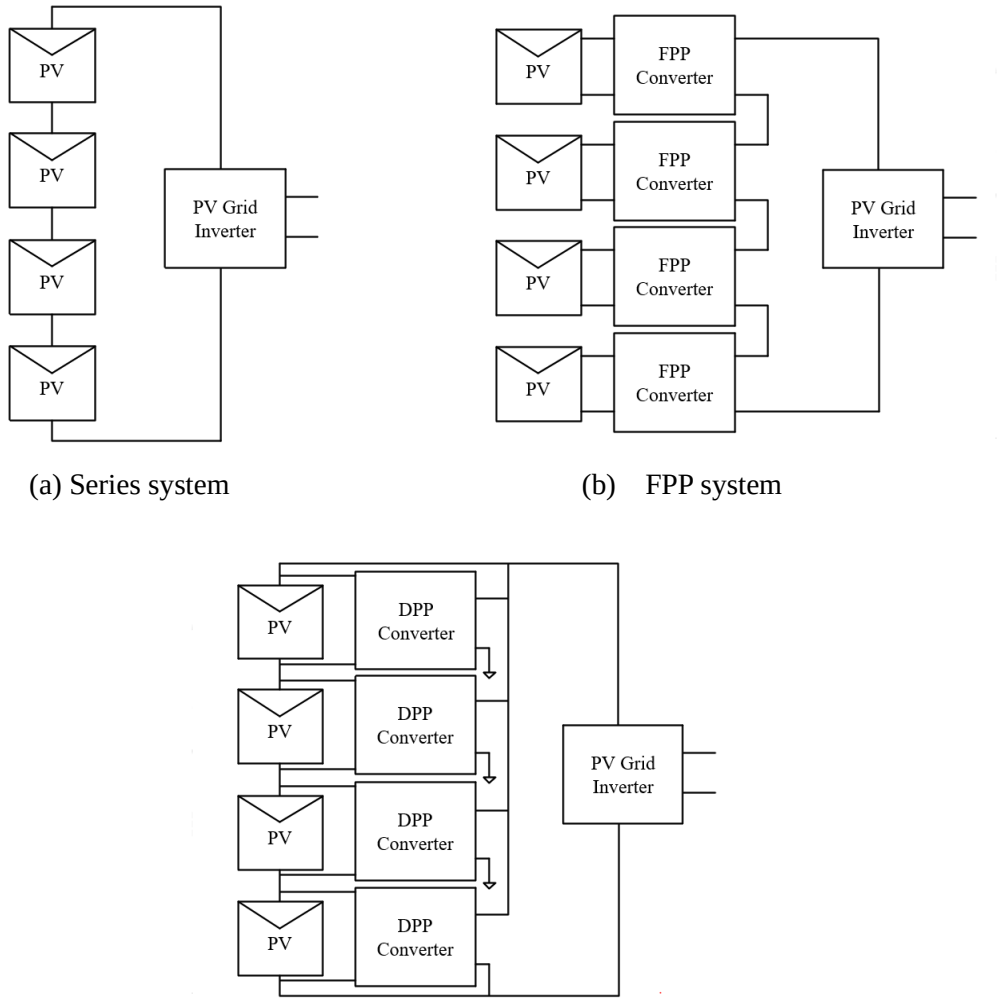

(a) Series system (b) FPP system

(c) DPP system

Fig. 1.1. PV connection system structure [14]

Thus, the voltage gain of the DPP converter is the number of series-connected PV modules. In other words, high voltage gain is required. Also, because of the connection structure of the DPP converter, the ground of the input port differs from the ground of the output port. It requires the galvanic-isolation characteristics of the DPP converter. To make other paths of the current, the DPP converter needs a bidirectional power flow function for the MPP operation of each PV module. The DPP system has a more complicated structure than the series connection system which consists of only PV Moules and parallel diodes. The DPP converter is connected to parallel per PV module, and several voltage and current sensors are configured. The configuration of such a DPP system causes problems of many failure situations such as converter active switch short, sensor malfunction, and short/open of converter input/output. These problems reduce the reliability of the DPP system. Therefore, the design of the DPP system should consider how to cope with failure situations [15].

ULSAN NATIONAL INSTITUTE OF
SCIENCE AND TECHNOLOGY

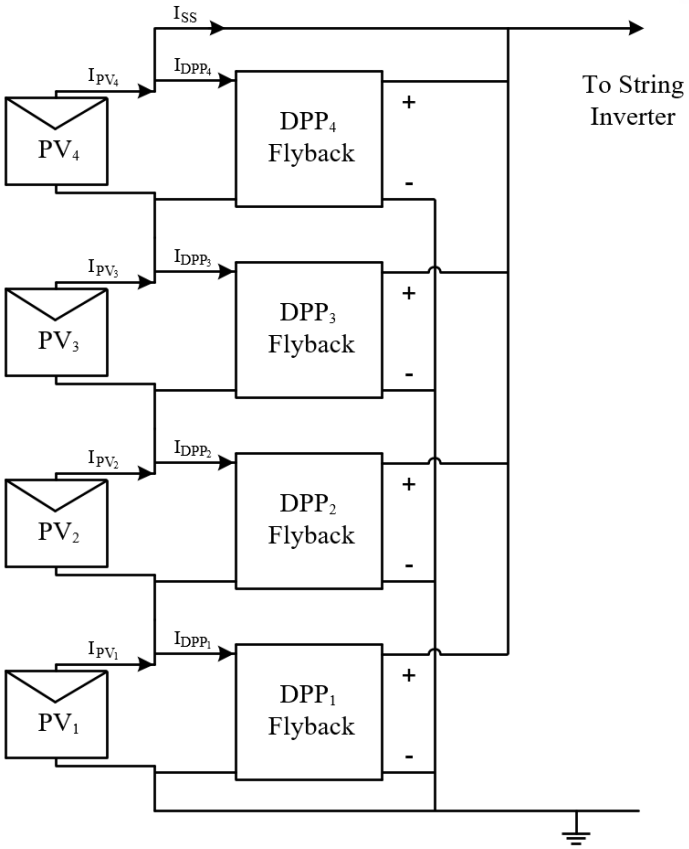

Fig. 1.2. PV-to-Bus structure differential power processing system [14]

This thesis introduces the algorithm and of the PV-to-Bus structure DPP system. Also, the design methodology of the bidirectional flyback converter suitable for this DPP structure and the development of a protection algorithm that can cope with the failure of the DPP system, and the verification through power hardware-in-the-loop (PHIL) simulation is introduced. The experimental testing is conducted to verify this system. As further work, an on/off algorithm suitable for DPP for several string diode PV modules is proposed and verified by simulation.

In Section II, description and power control algorithm of DPP system is described. The design methodology of the bidirectional flyback converter suitable for PV-to-Bus DPP structure is described in Section III. Section IV develops a protection algorithm to improve the reliability of the DPP system and verify the protection algorithm developed by modeling the DPP system and failure conditions through PHIL simulation. In Section V, as an indoor experimental method to confirm the developed DPP system performance, the PV emulation method which compensates the accuracy in MPP. The experimental results confirmed output power of the series connection and the DPP system under various partial shade conditions and results of PHIL simulation for verification protection algorithm in Section VI. As further work, an on/off algorithm suitable for DPP for several string diode PV modules is proposed and verified by simulation in Section VII. The last section concludes this thesis.

ULSAN NATIONAL INSTITUTE OF SCIENCE AND TECHNOLOGY

II. System Description of Differential Power Processing

The DPP system is capable of generating the maximum power of each panel even in partial shade conditions, and because only part of the generated power is delivered to the converter, the generation efficiency is high. Therefore, the DPP systems for PV applications are being highlighted as next-generation photovoltaic systems. In this section, the advantages of DPP, DPP architecture types and DPP algorithm are described.

2.1 Advantages of DPP System

Fig. 2.1 shows the types of PV DPP architecture [14]. PV-PV DPP architecture consists of one DPP converter between the PV modules as shown in Fig. 2.1(a). The number of DPP converters is always one less than the number of PV modules. Due to the structure of the DPP system, non-isolated bidirectional converters such as buck-boost converters are used. The DPP converters between PV modules enable power conversion between modules to compensate for deviations between modules. The PV-to- Bus DPP architecture consists of a DPP converter in parallel to the PV module as shown in Fig. 2.1(b). The number of DPP converters is always the same as the number of PV modules. Due to the structure of the DPP system, isolated bidirectional converters such as flyback converters are used. The DPP converters in parallel to PV modules enable power conversion between modules to compensate for deviations between modules.

Therefore, the DPP system of these structures is capable of generating a maximum power point of each panel, unlike the series connection system in which the amount of power is reduced in partial shade

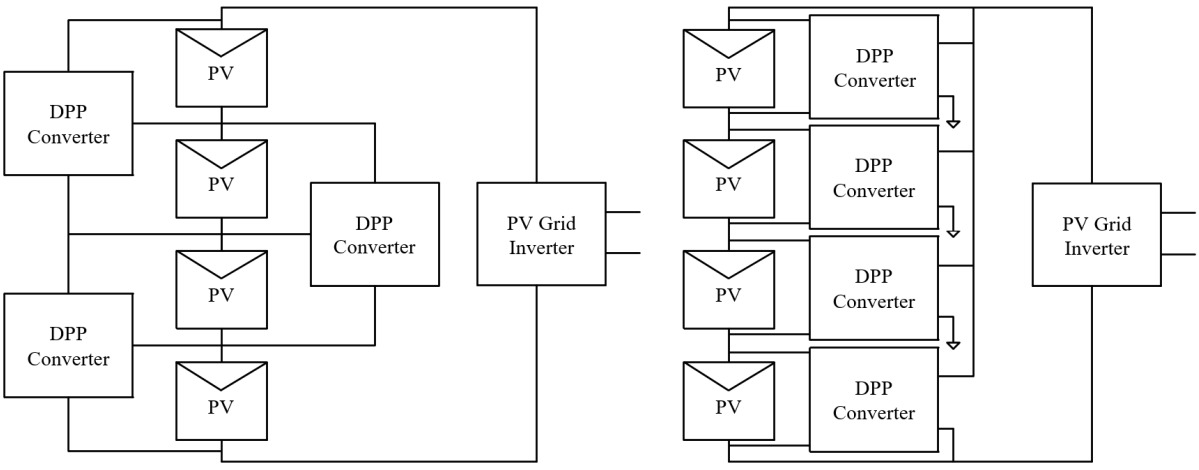

(a) PV-PV DPP architecture (b) PV-to-Bus DPP architecture

Fig. 2.1. PV DPP architecture types [14]

ULSAN NATIONAL INSTITUTE OF
SCIENCE AND TECHNOLOGY

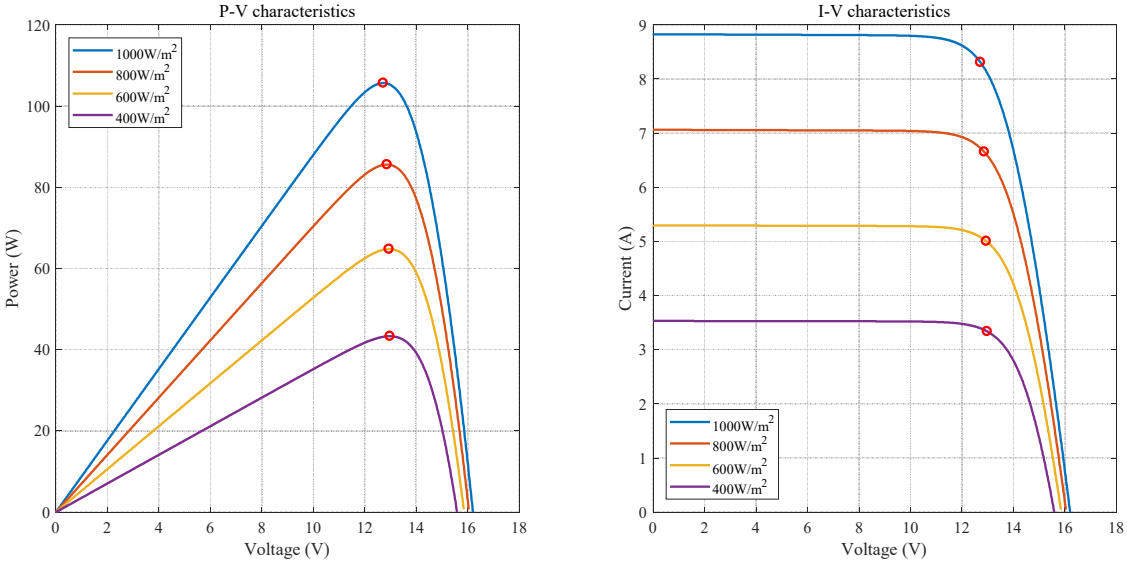

(a) *P-V* characteristic curve

(b) *I-V* characteristic curve

Fig. 2.2. PV characteristic curves

condition. In addition, unlike the FPP system in which all the generated power is delivered to the converter, only a part of the generated power is delivered to the converter to compensate for the deviation of each panel. This can reduce converter power capacity and losses in the converter. Because of these advantages, the DPP system is regarded as a more advanced photovoltaic power generation system, and a lot of research is being conducted on the DPP system.

2.2 DPP Algorithm

The DPP algorithm allows each PV module to generate at its own MPP under any sunlight condition. Therefore, the DPP algorithm checks the status of each PV module and controls the DPP converter. Basically, the DPP algorithm generates a current reference command that must operate to control the converter. This chapter describes the types of DPP power control algorithms for PV-to-Bus architecture DPP and introduces the algorithms applied in this paper.

2.2.1 Voltage Balancing Algorithm

The characteristic curve of PV according to solar irradiance is shown in Fig. 2.2 [16]. As can be seen, the current of MPP has a different value depending on the amount of solar irradiance. On other hands, the voltage of MPP is almost the same according to various irradiance. The voltage balancing algorithm, a simple DPP algorithm, takes advantage of this characteristic of the PV module. Since the voltage of

ULSAN NATIONAL INSTITUTE OF SCIENCE AND TECHNOLOGY

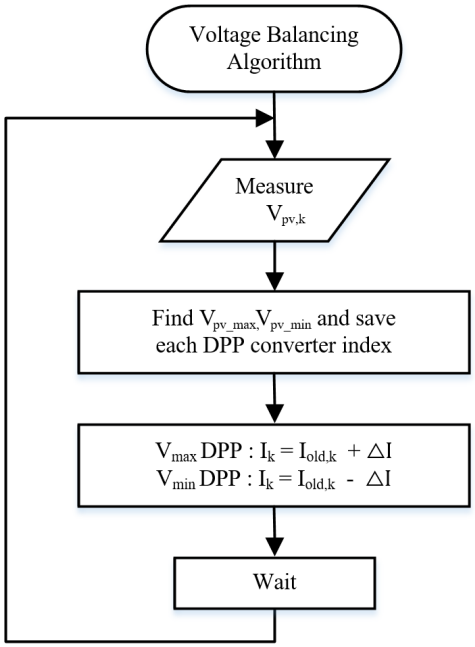

Fig. 2.3. Voltage balancing algorithm flow chart

MPP is almost constant even if the amount of solar irradiance changes, each panel generates power near MPP if the voltage of each PV module is set equal. Therefore, the DPP algorithm controls the DPP converter so that the voltage of each PV module is constant. The flow chart of the voltage balancing algorithm is shown in Fig. 2.3. After sensing the voltage information of all PV modules, control the PV voltages to be balanced by adjusting the current reference commands of the DPP converter of the highest and lowest voltage PV modules. The voltage balancing algorithm is simple and requires only a voltage sensor for PV module voltage and a current sensor for DPP converter current control to implement the algorithm. That is, only two sensors are required per PV module.

However, this algorithm only allows each PV module to generate power near the MPP, not at the correct MPP. This results in lower generating power compared to accurate MPP operation. Therefore, voltage balancing algorithms are used in applications requiring simple control and low production costs, or in combination with MPPT algorithms to quickly reach near MPP before accurate MPPT control.

2.2.2 MPPT Algorithm

The MPPT for the DPP algorithm is required because the voltage balancing algorithm alone does not allow each PV module to operate at the correct MPP. The MPPT algorithm uses perturbation & observation (P&O) to operate each PV module at the correct MPP [17]-[19]. This is a method of reaching the MPP by repeatedly changing the operating point of the PV and checking the output power. Fig. 2.4 shows a power maximize DPP algorithm flow chart using the MPPT. In this MPPT algorithm,

ULSAN NATIONAL INSTITUTE OF
SCIENCE AND TECHNOLOGY

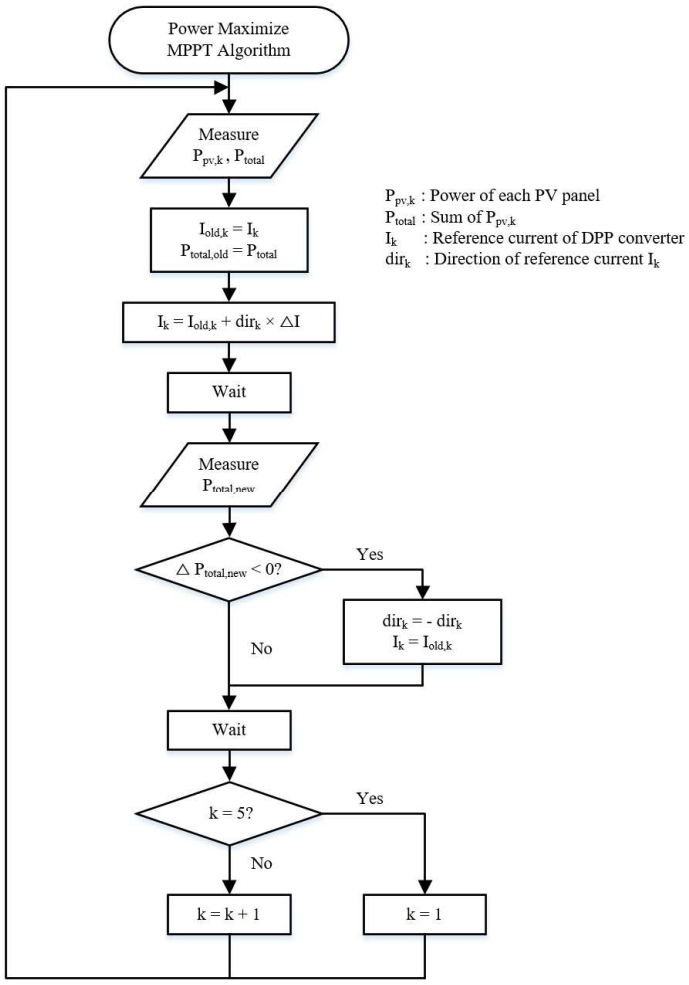

Fig. 2.4. Power maximize MPPT algorithm flow chart

each DPP converter operates by sequentially changing small currents in one direction. And then, the output power of the previous state is compared with the current output power. If the previous power is higher, change the current reference of the converter back and change the current in the opposite direction in the next perturbation. If the current power is higher, keep the reference current of the converter and change the current in the same direction in the next perturbation. This P&O method is applied to DPP to enable accurate MPP operation. This MPPT algorithm is more effective when used in conjunction with the voltage balancing algorithm described in the previous chapter. First, all PV modules reach a certain range of voltages using voltage balancing algorithms, and then MPPT algorithms are used to quickly reach the correct MPP. However, MPPT algorithms using P&O must check the output power, which increases the number of sensors in the DPP system. Fig. 2.5 shows the structure of the DPP system according to the number of sensors. Using only the voltage balancing algorithm, only 2n sensors can be used, as shown in Figure 2.5(a) (n is the number of PV modules). On the other hand, MPPT, which maximizes power, requires power information, requiring 2n + 1 or 3n sensors as shown in Fig. 2.5 (b),(c). Therefore, the MPPT algorithm that maximizes the power can

ULSAN NATIONAL INSTITUTE OF SCIENCE AND TECHNOLOGY

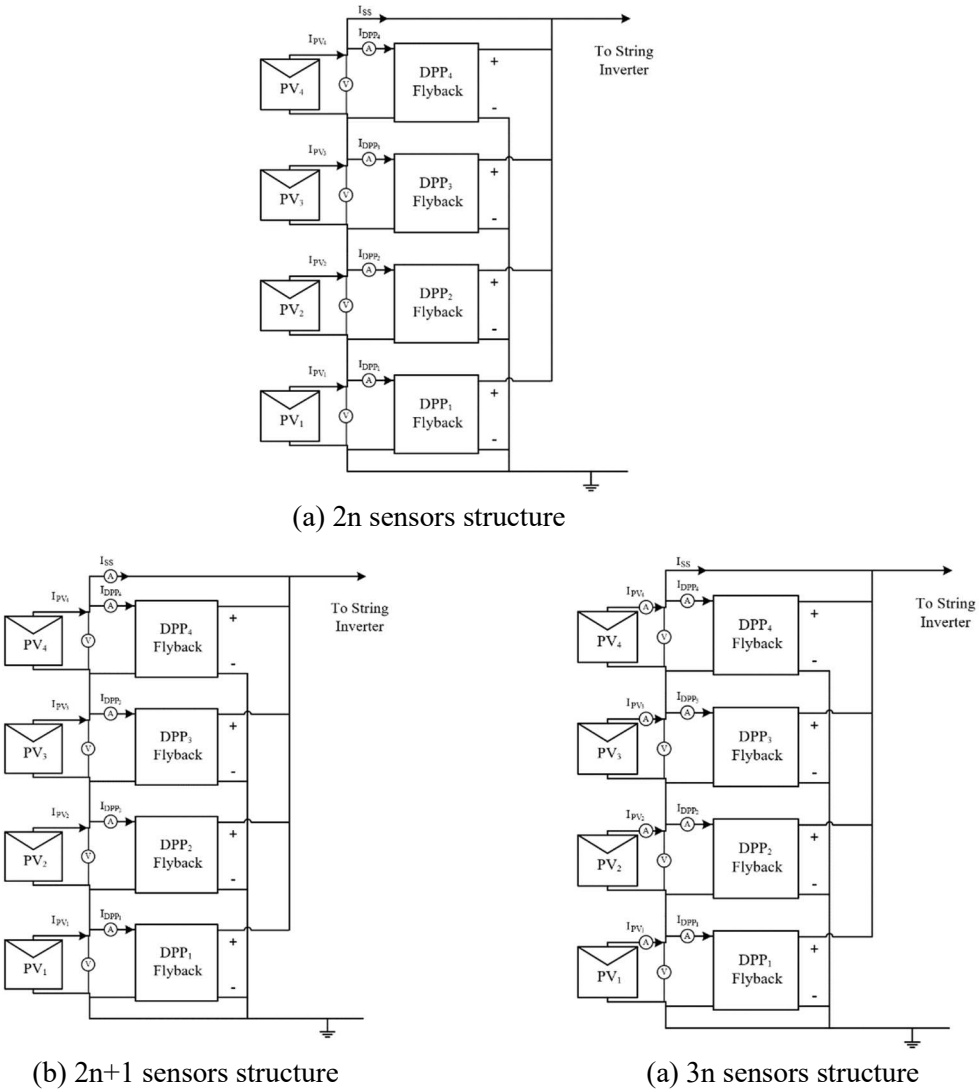

(a) 2n sensors structure

(b) 2n+1 sensors structure

(a) 3n sensors structure

Fig. 2.5. DPP system structure according to the number of sensors

operate the PV module in the correct MPP, but the system becomes more complicated and the system configuration cost increases.

To solve this shortcoming, total voltages maximize the MPPT algorithm has been proposed that enable accurate MPP operation and require no additional sensors [20]. The principle of the total voltage maximized algorithm is simple. In general, the DPP system has a grid-connected MPPT inverter connected to the output as shown in Fig. 2.1. Therefore, the MPPT of the DPP system and the MPPT of the PV inverter are simultaneously performed. If the MPPT of the DPP system is driven much faster than the MPPT of the PV inverter, it can be assumed that the output string current of the DPP system is constant. Since the current is assumed to be constant, maximizing the total voltage will eventually operate the PV at its MPP. However, due to the output characteristics of the PV, just increasing voltage does not ensure maximum power, so the voltage maximizer algorithm should always be used with the

ULSAN NATIONAL INSTITUTE OF
SCIENCE AND TECHNOLOGY

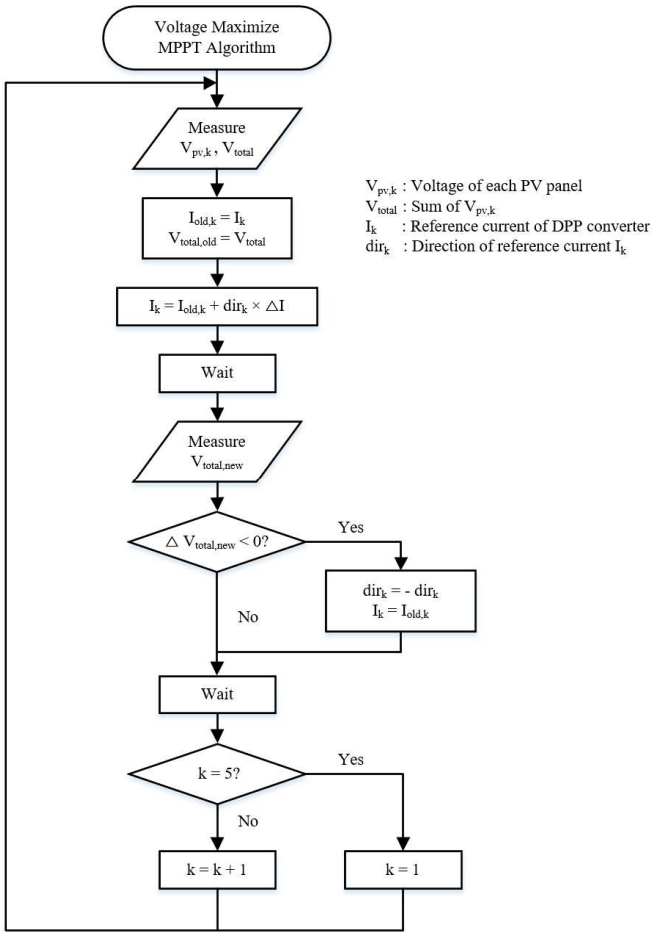

Fig. 2.6. Total voltage maximizes MPPT algorithm flow chart [20]

voltage balancing algorithm. That is, all PV modules enter the voltage range using the voltage balancing algorithm and operate near the MPP, and then operate at the correct MPP using the voltage maximize algorithm. Fig. 2.6 shows a flow chart of the total voltage maximize MPPT algorithm. Fig. 2.6 shows a flow diagram of the total voltage maximized MPPT algorithm. Like the power maximized algorithm, it uses P&O to converge on the MPP. It only changes from maximizing power to maximizing voltage. In conclusion, if the combination of the voltage balancing algorithm and the total voltage Maximized MPPT algorithm is used, the DPP algorithm can be performed using only 2n sensors as shown in Fig. 2.5 (a), which does not require additional sensors. Also, accurate MPP operation of each PV module is possible for maximum power production. In this thesis, the DPP system is configured using the proposed combination of the voltage balancing algorithm and the total voltage maximize MPPT algorithm.

ULSAN NATIONAL INSTITUTE OF
SCIENCE AND TECHNOLOGY

III. Design Methodology of Bidirectional Flyback Converter for DPP

DPP systems can adjust the current in each panel by a differential converter connected in parallel with the panel in case of power unbalance between the panels. Therefore, even if the power unbalances occurs between panels, each panel operates at an MPP, and high system efficiency can be obtained. However, since the performance of the DPP system is influenced by the performance of the differential converter, it is important to design a differential converter that achieves high power transfer efficiency and reliable operation. Moreover, the differential converter requires bidirectional power transfer function, high power density, primary and secondary isolation characteristics, and high-power conversion efficiency. In this paper, a design methodology of the bidirectional flyback converter is proposed which is suitable for a differential converter for the PV-to-Bus structure DPP module. The validity of the proposed design methodology is verified using a 25.6-W bidirectional flyback converter prototype.

3.1 Bidirectional Flyback Converter Topology

3.1.1 Features of PV-to-Bus Structure Differential Converter

In a PV-to-bus structure DPP system, each panel has a differential converter connected in parallel and output stage of the converter is connected to output stage of the PV module series as shown in Fig. 2.1(b). The connection structure of this differential converter forms the path of the series string current. Therefore, when partial shading occurs between PV modules, the differential converter of the PV module with a large amount of power generation operates in the forward direction, and the differential converter of the PV module with a small amount of power generation operates in the reverse direction to operate in each PV module at MPP. This causes an increase in power generation of the photovoltaic system [10].

The requirements of the differential converter of the PV-to-Bus DPP system to meet this structure and operation are as follows. The requirements of the differential converter to meet this structure and operation are as follows. First, bidirectional operation must be possible for maximum power point operation of each PV modules. Secondly, since the converter input is connected to one panel and the converter output is connected to the output terminal of the series connection of the panel, the boost ratio is as high as the number of panels to be connected. Third, because each differential converter is connected in series and the output is tied in parallel, the differential converter must be isolated between primary and secondary. Finally, a topology with a simple circuit structure is advantageous because several converters are used as modules. Therefore, bidirectional flyback converter is selected as a power converter for PV-to-Bus DPP module.

ULSAN NATIONAL INSTITUTE OF
SCIENCE AND TECHNOLOGY

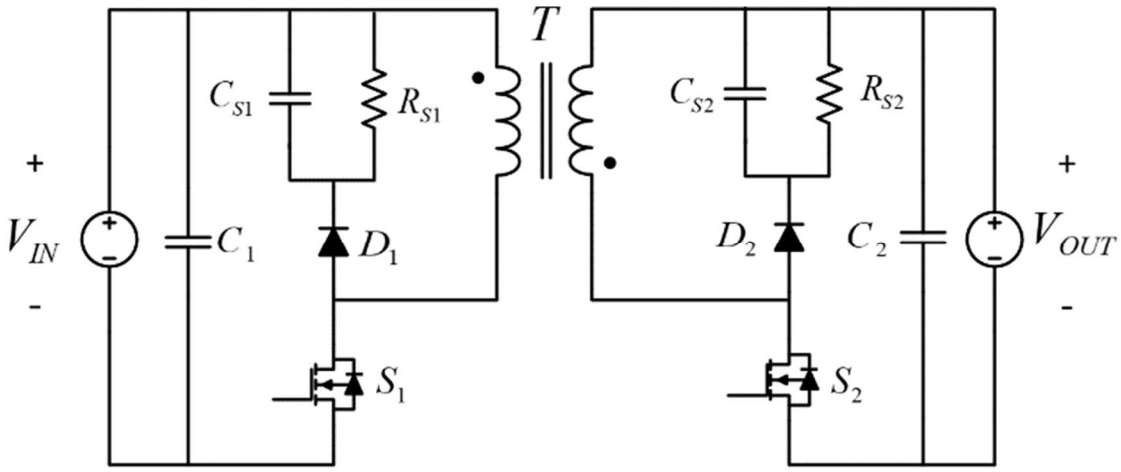

Fig. 3.1. Schematic of bidirectional flyback converter

3.1.2 Circuit Structure of Bidirectional Flyback Converter

Fig 3.1 shows the circuit structure of the bidirectional flyback converter for PV-to-Bus DPP module. T represents the main transformer of the converter and S_1 and S_2 are the main switch of the converter. The turn ratio of the transformer T is n. R_{S1}, C_{S1}, and D_1 configure the RCD snubber circuit which protects primary switch S_1 from high voltage spike that occurs when primary switch S_1 turns off. Similarly, R_{S2}, C_{S2}, and D_2 configure the RCD snubber circuit which protects secondary switch S_2 from high voltage spike that occurs when secondary switch S_2 turns off. Therefore, it can be confirmed that the bidirectional flyback converter can be bidirectional power transfer, has electrical isolation characteristics, has a high voltage gain, and has a simple structure.

3.1.3 Design Consideration

In a flyback converter, the power conversion efficiency is affected by the magnetizing inductance of the transformer. The magnetizing inductance changes the waveform of the switch current on the input side, causing the effective and maximum magnitudes of the current to fluctuate, causing changes in conduction loss and efficiency even at the same amount of power. The magnetizing inductance also determines the continuous and discontinuous conduction modes in flyback converter operation. Therefore, magnetizing inductance design is an essential consideration in the design of flyback converters. Unlike the conventional flyback converter, the bidirectional flyback converter circuit shown in Fig. 3.1 consists of a switch, not a diode, on the output side for bidirectional operation. During power conversion, the switch on the output side is turned off and operates only as an anti-parallel diode. In general, the anti-parallel diode of the switch has poor reverse recovery characteristics [21]. Therefore,

ULSAN NATIONAL INSTITUTE OF
SCIENCE AND TECHNOLOGY

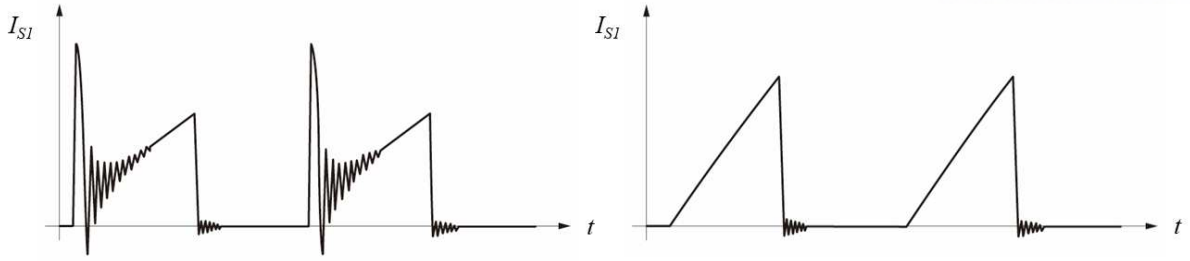

(a) Continuous conduction mode (b) Discontinuous conduction mode

Fig. 3.2. Theoretical waveforms of input switch's drain current [23]

if the input side switch is turned on in the continuous conduction mode when current flows through the output side antiparallel diode, reverse recovery loss occurs on the output side antiparallel diode, and as shown in Fig. 3.2, large ripple occurs [22,23]. This causes the problem of increasing the output voltage ripple and increasing the conduction loss of the converter by increasing the effective value of the input switch current. Therefore, it is advantageous to operate in discontinuous conduction mode, in which the input switch turns on when no current flows in the anti-parallel diode on the output side, and it is necessary to design a magnetizing inductance in which the converter can operate in discontinuous conduction mode.

Differential power processing system drives the differential converters in the event of power imbalance between panels, allowing each panel to operate at its maximum power point, increasing the efficiency of the overall system. Therefore, if the efficiency of the differential converter is low, the loss caused by driving the converter will lower the overall power generation efficiency. Therefore, it is important to design a differential converter with high efficiency in bidirectional power conversion. When the power deviation between the solar panels is large, the power generation of the entire system is lowered and the power delivered to the differential converter is larger, so the loss in the differential converter has a greater effect on the overall system efficiency. Therefore, the design of the differential converter is advantageous in terms of reducing power loss with respect to the total amount of generation at uneven solar irradiance because it is designed to focus on efficiency at rated load.

3.2 Proposed Design Methodology

3.2.1 Conduction Mode Selection

According to the design considerations in the previous chapter, the DPP flyback converter should be designed to operate in discontinuous conduction mode and should be designed with a focus on efficiency at rated load. Therefore, the efficiency of the converter is analyzed by calculating the loss components according to the magnetizing inductance in the discontinuous conduction mode under the

ULSAN NATIONAL INSTITUTE OF SCIENCE AND TECHNOLOGY

rated load. The design equation for the magnetizing inductance (Lm) of a flyback converter transformer operating in discontinuous conduction mode is as follows.

$$L_m = \frac{(V_{in} D)^2}{2 P_{in} f_s} \tag{1}$$

Where V_{in} is the input voltage, P_{in} is the input power, f_s is the switching frequency, and D is the duty ratio. V_{in}, P_{in}, and f_s are determined by the requirements of the converter design. Therefore, the magnetization inductance equation can be expressed as a function of D at the rated load in the discontinuous current mode.

Each power dissipation component of a bidirectional flyback converter can be expressed as a function of the maximum and effective values of the input switch current that changes as the magnetizing inductance changes. The equation of the maximum value and the effective value of the input switch current is as follows.

$$I_{peak} = \frac{2}{D} \times I_{mean} \tag{2}$$

$$I_{rms} = \sqrt{\int_0^D \left(\frac{I_{peak}}{D} t \right)^2 dt} = \frac{2 I_{mean}}{D} \sqrt{\frac{D}{3}} \tag{3}$$

Where I_{peak} is the maximum value of the input switch current, I_{rms} is the effective value of the input switch current, and I_{mean} is the average value of the input switch current at rated load. Since I_{mean} is determined by the design requirements, the maximum and effective values of the switch currents in equation (2) and (3) are functions of D. Therefore, by substituting equation (1) into equation (2) and (3), the equation of the maximum value and the effective value of the switch current is expressed as follows.

$$I_{rms} = \sqrt{\frac{2 P_{in}}{L_m f_s}} \tag{4}$$

$$I_{rms} = \sqrt{\frac{2 P_{in} \sqrt{2 P_{in} L_m f_s}}{3 V_{in} L_m f_s}} \tag{5}$$

At rated load, P_{in}, I_{mean}, and f_s are constants determined by the design requirements, so the maximum and effective values of the input switch current are described as a function of the magnetizing inductance. To select the magnetizing inductance, the power loss graph is calculated by calculating the primary and secondary snubber loss, input switch conduction loss, switching loss, transformer loss, and output diode conduction loss according to the magnetizing inductance. Each power loss component is described as a function of the magnetizing inductance in the form of the rms and maximum values of the current. The formula of each power loss component is as follows.

ULSAN NATIONAL INSTITUTE OF SCIENCE AND TECHNOLOGY

$$P_{Sn,pri} = \frac{1}{2} L_{lk} {I_{peak}}^2 \frac{V_{sn1}}{V_{sn1} - \frac{V_{out}}{n}} f_s \tag{6}$$

$$P_{Sn,\sec} = \frac{1}{2} \left(\frac{V_{in} n}{V_{sn2}} \right)^2 L_{lk} {I_{peak}}^2 \frac{V_{sn2}}{V_{sn2} - V_{in} n} f_s \tag{7}$$

$$P_{Swithing} = \frac{1}{2} I_{peak} \left(V_{in} + \frac{V_{out}}{n} \right) f_s \, t_{off} \tag{8}$$

$$P_{Conduction,switch} = {I_{rms}}^2 R_{ds} \tag{9}$$

$$P_{Copper} = {I_{rms}}^2 R_{copper} \tag{10}$$

$$P_{Diode} = V_f \frac{I_{mean}}{n} \tag{11}$$

Where $P_{sn,pri}$ is the primary snubber loss, $P_{sn,sec}$ is the secondary snubber loss, $P_{switching}$ is the switching loss, $P_{conduction,switch}$ is the input switch conduction loss, P_{copper} is the transformer copper loss, P_{diode} is the output diode conduction loss, and R_{ds} is on resistance of the switch, L_{lk} is the leakage inductance, R_{copper} is the transformer resistance, V_{sn1} is the primary side snubber voltage, V_{sn2} is the secondary side snubber voltage, n is the transformer turn ratio, V_f is the diode threshold voltage, and t_{off} is the turn-off time.

Fig. 3.3 shows power loss analysis curves according to magnetizing inductance under the DCM in the experimental conditions of Table I. The calculated loss components are snubber loss, copper loss, diode conduction loss, switch conduction loss, switching loss and core loss. In this analysis, the turn ratio of the transformer is fixed to the voltage ratio of the converter. As shown in Fig. 3.3, as the magnetizing inductance value increases, the maximum value and the effective value of the input switch current decrease, and the loss of the converter decreases. Therefore, the magnetizing inductance of the bidirectional flyback converter is designed to operate in the boundary conduction mode (BCM) having the largest magnetizing inductance in the DCM section [24].

3.2.2 Magnetizing Inductance Design

The magnetizing inductance with the minimum loss is designed by calculating the loss according to the magnetizing inductance in the BCM operating section under the rated load. According to equation (1) and (12) in BCM operation at rated load, if all other parameters except for the magnetizing inductance, duty, and turn ratio are constant, the magnetizing inductance, duty, and turn ratio are determined at the same time. The loss according to the magnetizing inductance of the bidirectional flyback converter under the rated load in the experimental conditions of Table I as shown in Fig. 3.4. From the results in Fig. 3.4, for both forward and backward operation, the primary magnetizing inductance value is about 14.7μH which is the minimum loss. At this magnetizing inductance value,

ULSAN NATIONAL INSTITUTE OF SCIENCE AND TECHNOLOGY

TABLE I EXPERIMENTAL DESIGN CONDITION

Symbol	Meaning	Value
V_{in}	Input Voltage	14.8 V
V_{out}	Output Voltage	59.2 V
f_{sw}	Switching Frequency	100 kHz
I_{in}	Input Current	1.7 A
P_{in}	Input Power	25.16 W

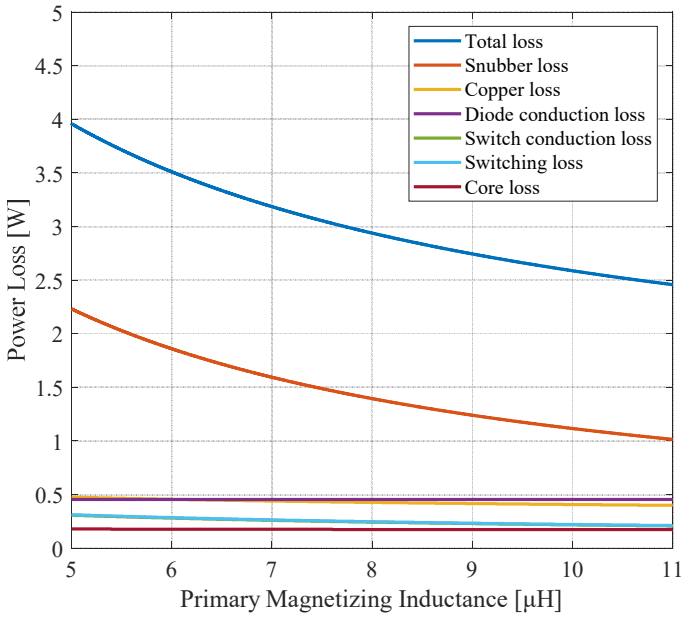

(a) Forward operation

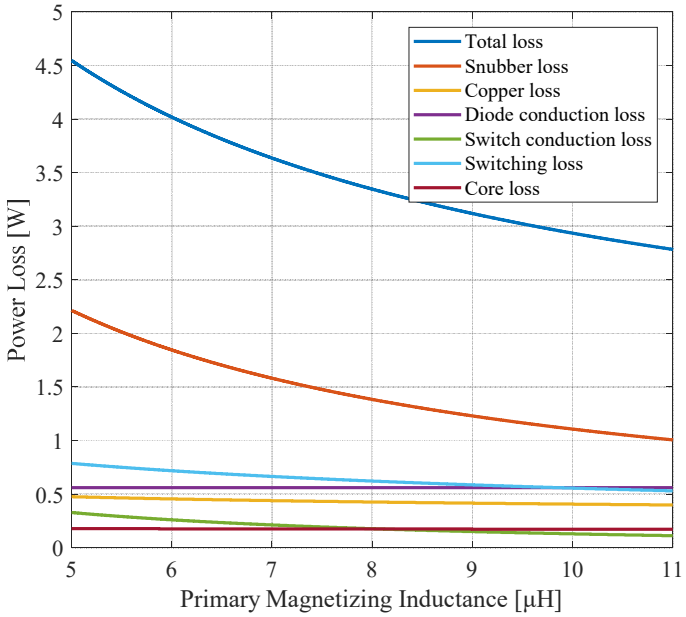

(b) Backward operation

Fig. 3.3. Power loss analysis curve under DCM when turn ratio is 4

ULSAN NATIONAL INSTITUTE OF
SCIENCE AND TECHNOLOGY

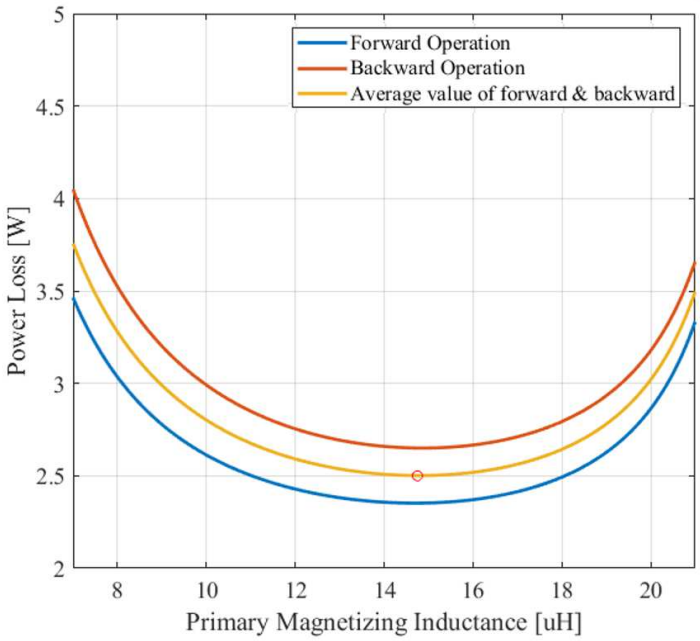

Fig. 3.4. Power loss analysis curves according to L_m under BCM condition with turn ratio variation

$$\frac{V_{out}}{V_{in}} = \frac{D}{1-D} n \tag{12}$$

the forward duty value is about 0.58, and the turn ratio of the transformer is about 2.88.

Table II shows the power loss and efficiency of each component of the bidirectional flyback converter when the magnetizing inductance value of 14.7uH with the smallest bidirectional loss is selected. As can be seen in Table II, a total power loss of about 2.4 W for forward operation and about 2.7 W for backward operation is expected. The forward operation efficiency is higher than the backward operation efficiency. This difference is caused by a large loss of the output diode in the reverse operation in which the diode is conducted at the low voltage side and switching loss. The other loss components except for diode conduction loss have similar values in forward and backward operation. In addition, since the on-resistance is low and the turn-off time is short when using the condition value of the power switch, the snubber loss is larger than the conduction loss and switching loss in both bidirectional power conversion operations. The analyzed efficiency is about 90.56% in the forward direction and about 89.40% in the backward direction.

3.3 Experimental Verification

In this chapter, the proposed efficiency and design method are experimentally verified by implementing a 25 W prototype. In the experiment, the design margin is set to the magnetizing inductance value due to the loss of circuit, parasitic component, inductance measurement error, and change of converter parameter in time domain. Therefore, in this experiment, the magnetizing

ULSAN NATIONAL INSTITUTE OF SCIENCE AND TECHNOLOGY

TABLE II BIDIRECTIONAL FLYBACK LOSS ANALYSIS

Loss component	Meaning	Value	Unit
Snubber loss	0.928	0.830	*W*
Copper loss	0.400	0.400	*W*
Diode conduction loss	0.454	0.562	*W*
Switch conduction loss	0.179	0.136	*W*
Switching loss	0.217	0.541	*W*
Core loss	0.197	0.197	*W*
Total loss	2.375	2.666	*W*
Efficiency	90.56	89.40	*%*

TABLE III BIDIRECTIONAL FLYBACK DESIGN PARAMETERS

Parameter	Mark	Value	Unit
Input voltage	V_{in}	14.8	*V*
Input power	P_{in}	25.16	*W*
Output voltage	V_{out}	59.2	*V*
Turns ratio	n	2.88	-
Primary snubber capacitance	C_{S1}	100	*nF*
Secondary snubber capacitance	C_{S2}	5	*nF*
Primary snubber resistance	R_{S1}	2	*kΩ*
Secondary snubber resistance	R_{S2}	40	*kΩ*
Magnetizing inductance	L_m	12.6	*μH*
Leakage inductance	L_{lk}	0.26	*μH*
Switching frequency	f_s	100	*kHz*

inductance of 12.6 μH was selected considering the design margin. Table III shows the prototype values obtained according to the converter design scheme proposed in Chapter 3.2. Fig. 3.5 shows the prototype of the bidirectional flyback converter and the experimental setup.

Fig. 3.6 shows the experimental waveforms of forward and backward operation at the rated load of a bidirectional flyback converter. As can be seen from the input current waveform of the switch, it can be seen that it operates in the discontinuous conduction mode at the rated load in both the forward operation and the backward operation. Although high voltage spikes exist in the switch voltage, the snubber loss is tremendous, and the device designed to reduce the magnitude of the voltage-clamped by the RCD snubber and to withstand the high voltage is used to improve efficiency. However, this can be adjusted according to the design requirements of the DPP system to be applied.

Fig. 3.7 is a graph of the full load efficiency of a bidirectional flyback converter. Efficiency at 25 W rated load is measured at 90.3% for forward and 89.3% for backward. This is similar to the calculated efficiency of 90.56% forward and 89.40 % backward. In addition, the difference between the forward

ULSAN NATIONAL INSTITUTE OF SCIENCE AND TECHNOLOGY

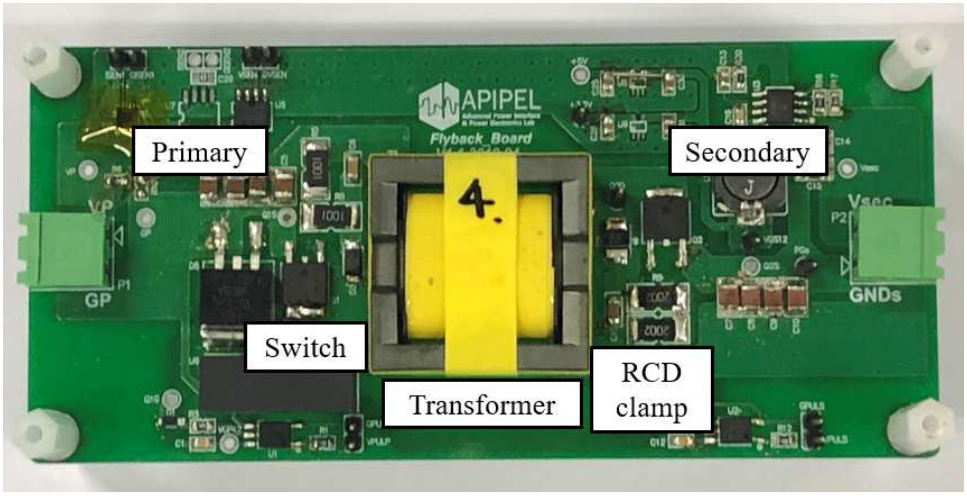

(a) Bidirectional flyback converter prototype

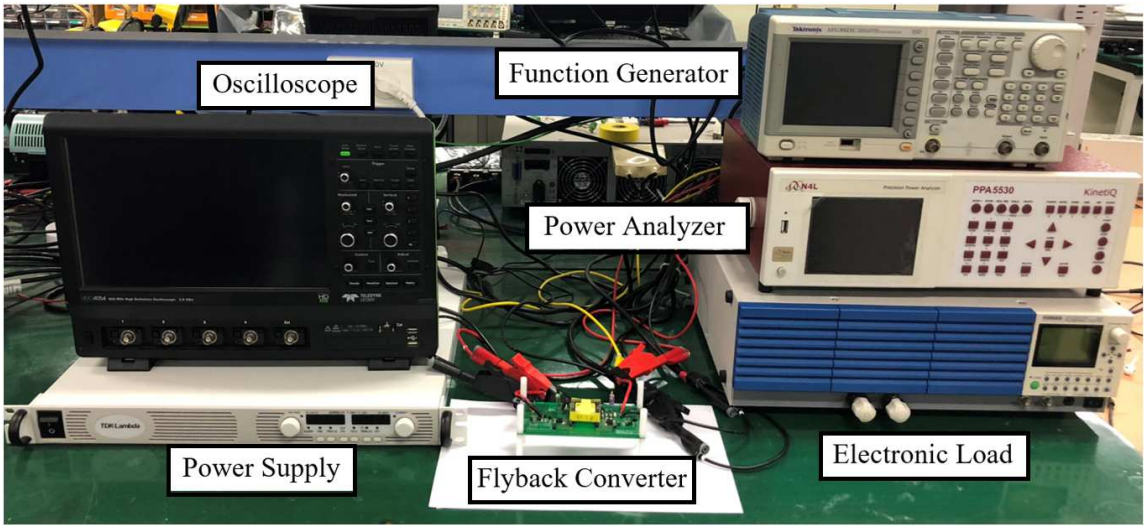

(b) Experimental setup

Fig. 3.5. Photographs of converter experiments

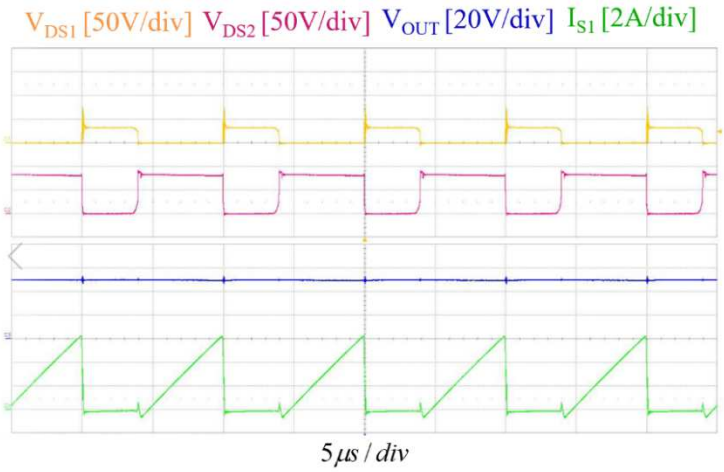

(a) Forward operation

ULSAN NATIONAL INSTITUTE OF SCIENCE AND TECHNOLOGY

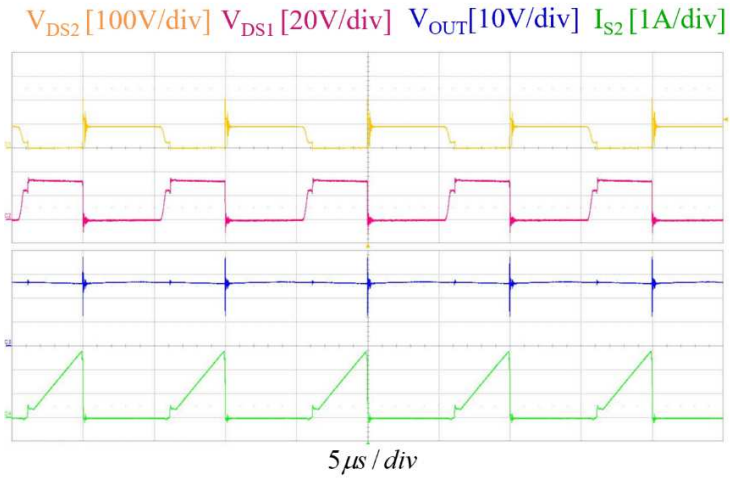

(b) Backward operation

Fig. 3.6. Theoretical waveforms of input switch's drain current

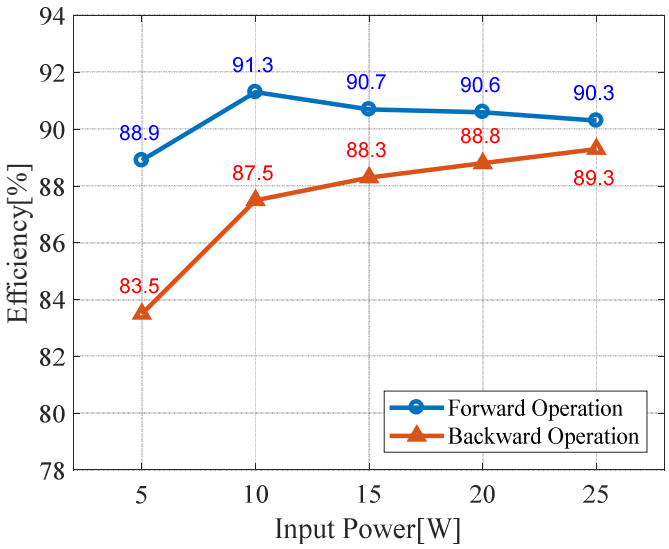

Fig. 3.7. Power conversion efficiency

operation and the reverse operation shows that the forward efficiency is higher than the reverse efficiency, as analyzed in Chapter 3.2, and the difference is about 1%. Thus, the accuracy of the theoretically calculated loss analysis was experimentally verified and the validity of the optimal magnetizing inductance selection method presented from the theoretical analysis was verified.

In this chapter, a design methodology of bidirectional flyback converter for PV-to-bus structure DPP module is presented. According to the characteristics and design considerations of the proposed bidirectional flyback converter, the design methodology of selecting the magnetizing inductance value with minimum loss is proposed by calculating the loss in the boundary conduction mode. The validity of the presented design method is verified by comparing the theoretical analysis and the results with the prototype of the converter manufactured by the proposed design method. Also, it is confirmed that the forward efficiency is 90.3% and the backward efficiency is 89.3% at the rated load of 25.16 W.

ULSAN NATIONAL INSTITUTE OF SCIENCE AND TECHNOLOGY

IV. In-Laboratory Test Method of Power Generation from PV Module

To demonstrate the performance of the DPP system, the experimental verifications of the PV power system circuitry are required. Conventional methods use light sources or outdoor experiments. The light source can support to perform the indoor experiments, which is an easy way to implement the desired experimental conditions (e.g., partial shading condition). However, the light source consumes a lot of electric power to obtain irradiance enough. In addition, the light source equipment requires high cost and large installation space to construct the experimental set-up. The outdoor experiment is the most direct verification method; however, it is affected by the weather conditions. Besides, it is difficult to maintain uniform irradiance conditions and to obtain desired experimental conditions perfectly.

To solve this problem, PV emulation methods have been proposed. They do not require expensive equipment and large space. It is possible to perform indoor experiments in the laboratory scale and easily provides the desired experimental conditions. Conventional PV emulation method connects DC power supply in parallel to a PV panel as shown in Fig. 4.1(a). It can simply emulate the nonlinear characteristics of the PV panel only using the PV panel and the DC power source [25]. This method does not require simulating or measuring the PV modules in advance to obtain the PV characteristics. However, its accuracy is lower than that of the previous methods because the emulated PV voltage is higher than that of the real PV module. Consequently, it cannot validate the performance of the PV power generation system with desired accuracy, especially at the MPP.

In this chapter, a novel PV emulation method which can improve the accuracy of the emulated output voltage at the MPP is proposed as shown in Fig. 4.1(b). It only consists of the PV module, the DC power source, and an additional resistor. Using the proposed method, to demonstrate the performance of the DPP system can be easily emulated without outdoor experiment. Besides it has high accuracy nearby the MPP so that it can easily verify the performance of the DPP systems which operate at the MPP. The proposed PV emulation method is evaluated in terms of the accuracy of the output voltage compared with the outdoor experiments and the conventional emulation methods.

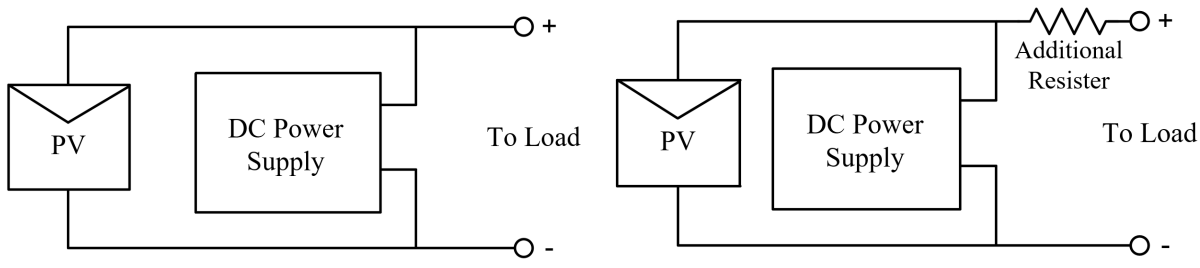

(a) Conventional method (b) Proposed method

Fig. 4.1. Laboratory emulation method of the PV module using DC power supply

ULSAN NATIONAL INSTITUTE OF SCIENCE AND TECHNOLOGY

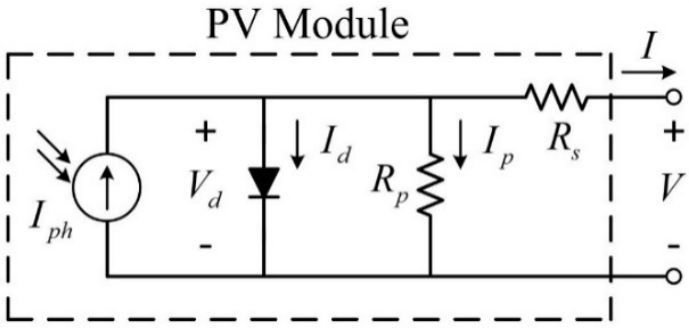

Fig. 4.2. Equivalent electrical circuit of the single-diode PV model.

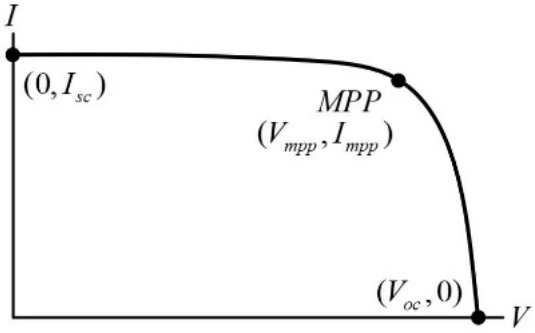

Fig. 4.3. Non-linear characteristic *I*-*V* curve of the PV modules.

4.1 Conventional Test Method

4.1.1 Single Diode PV Model

Although there are many PV models, a single diode PV model has been widely used in previous studies because it is simple and has high accuracy. The equivalent circuit of the single diode PV model is shown in Fig. 4.2. The characteristics of the output voltage V and output current I in the single diode PV model are represented as follows:

$$V_d = V + IR_s \tag{16}$$

$$\begin{aligned} I &= I_{ph} - I_d - I_p \\ &= I_{ph} - I_o\left[\exp\left(\frac{V_d}{V_t}\right) - 1\right] - \frac{V_d}{R_p} \\ &= I_{ph} - I_o\left[\exp\left(\frac{V + IR_s}{V_t}\right) - 1\right] - \frac{V + IR_s}{R_p} \end{aligned} \tag{17}$$

where V_d and I_d is the equivalent diode voltage and current, respectively, I_{ph} is the photocurrent generated by light hitting the PV panel, I_p is the current passing through the equivalent parallel resistor, I_o is the saturation current, V_t is the thermal voltage, R_s is the equivalent series resistance, and R_p is the equivalent parallel resistance [26].

ULSAN NATIONAL INSTITUTE OF SCIENCE AND TECHNOLOGY

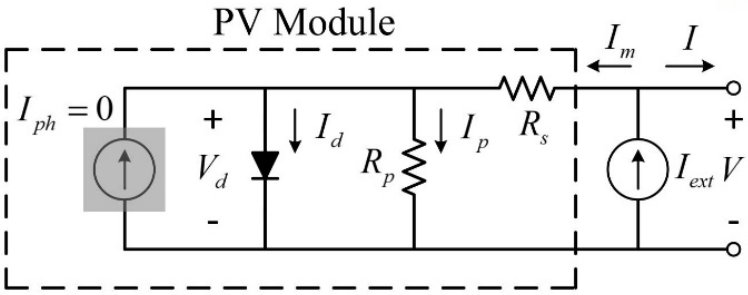

Fig. 4.4. Equivalent circuit of conventional emulation method.

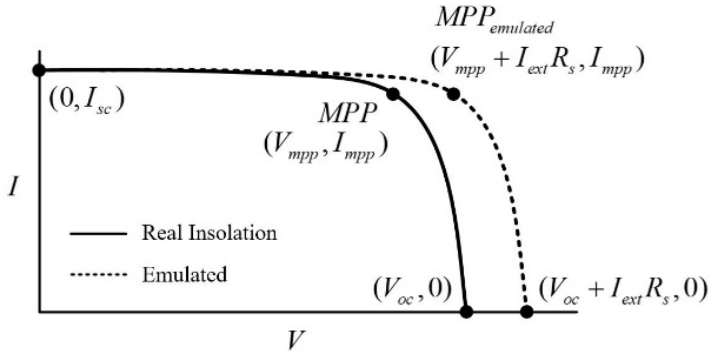

Fig. 4.5. *I-V* curve of the real insolation and conventional emulation.

According to (16) and (17), when the equivalent diode voltage of V_d increases (with high diode current), the output current decreases. In addition, when V_d decreases (with low diode current), the output current increases. Thus, the PV modules have a non-linear characteristic as shown in Fig. 4.3.

4.1.2 In-Lab PV Emulation

To emulate the non-linear characteristics of the PV modules, the conventional PV emulation methods use the external current source connected to the PV module's output port as show in Fig. 4.1(a). The equivalent electrical circuit of the conventional PV emulation method is shown in Fig. 4.4. The procedures of using the conventional PV emulator is as follows: First, block the PV panel from external light to set the internal production current zero. After that, the external current source is connected to the output of the PV panel to replace the current generated by the light. The value of the current source is set to the short circuit current generated by target irradiance to be emulated. Then, the PV characteristics are emulated according to the internal nonlinear characteristics of the PV panel itself. The characteristics of the output voltage V and the output current I are represented as follows:

$$V_d = V - I_m R_s \tag{18}$$

where I_{ext} is the current of the external current source, I_m is the current flowing inside of the PV panel. The diode voltage equation (3) of the emulation method is different from the actual PV internal diode equation

ULSAN NATIONAL INSTITUTE OF SCIENCE AND TECHNOLOGY

$$\begin{aligned} I &= I_{ext} - I_d - I_p \\ &= I_{ext} - I_o\left[\exp\left(\frac{V_d}{V_t}\right) - 1\right] - \frac{V_d}{R_p} \\ &= I_{ext} - I_o\left[\exp\left(\frac{V - I_m R_s}{V_t}\right) - 1\right] - \frac{V - I_m R_s}{R_p} \end{aligned} \tag{19}$$

(1). Since the threshold voltage characteristics of the equivalent diode are the same, the diode of the emulation method conducts at a higher output voltage than that of the real PV module. Thus, the PV characteristics of the higher output voltage are obtained as shown in Fig. 4.5. It causes accuracy issues in the PV emulation method. Therefore, the PV power generation system designed by the actual PV module operates at the higher voltage than the desired voltage. It cannot be accurately evaluated the exact performance of the target PV system.

To solve the accuracy problem of the conventional PV emulator, the reference of [28] configured an additional external voltage source connected to the emulator output in series to reduce the output voltage. However, it requires additional power supplies. Moreover, the magnitude of the voltage source should be tuned according to the operating condition to provide high accuracy of the emulator.

4.2 Proposed Test Method

According to the previous section, the difference between the real PV module and the conventional emulation method is the presence or absence of a resistor at the output stage. In the real PV module, the internal current generated by the sunlight passes through the series resistor R_s. However, in the conventional PV emulators, since the current source is configured externally, the output current does not pass the series resistor. This difference affects the equivalent diode voltage V_d, thus it causes accuracy problems. Inspired by above issue, the proposed PV emulator modifies the conventional PV emulator by connecting an additional series resister to the output port of the emulator as shown in Fig. 4.6.

When the additional series resistor is connected, the equivalent diode voltage of the conventional emulation method can be described by the following equation.

$$V_d = V + IR_s - I_m R_s \tag{20}$$

In (20), the IR_s term is added to the equivalent diode voltage equation. According to (20), following approximation is possible in the MPP where the current I_m entering the PV module is very small compared with the output current I.

$$V_d \simeq V + IR_s \, (I \gg I_m) \tag{21}$$

The approximation of (21) shows that the equivalent diode voltage of the proposed emulation method is equal to the equivalent diode equation of (16) for the real PV module operating at the MPP. Since the error of the equivalent diode voltage at the MPP can be compensated by using the proposed method, the

ULSAN NATIONAL INSTITUTE OF SCIENCE AND TECHNOLOGY

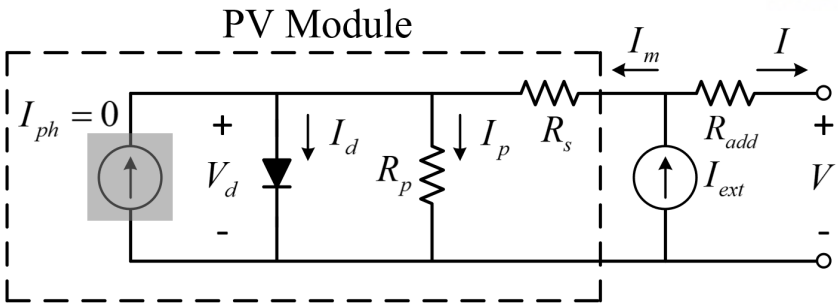

Fig. 4.6. Proposed in-laboratory emulation method of the PV module.

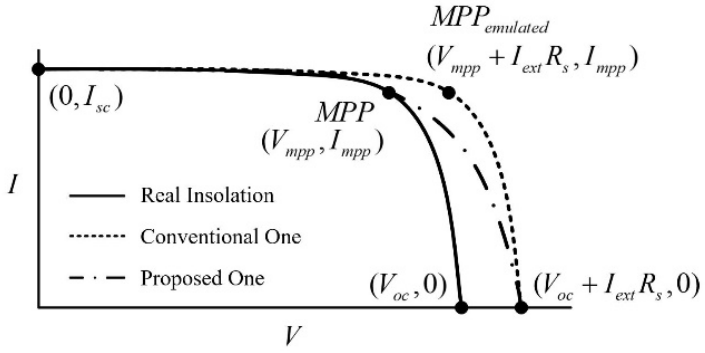

Fig. 4.7. *I-V* curves of the real PV module, conventional, and proposed emulation methods.

output voltage and current accuracy at the MPP are also improved. Therefore, as shown in Fig. 4.7, the current-voltage characteristic curve of the proposed emulation method shows improved accuracy at the MPP. Adjusting the additional series resistance can further improve the emulation accuracy at the MPP. It is assumed that the equivalent diode voltage of the actual PV module and the proposed emulation method are almost same at the MPP. The following voltage equation can be obtained by (16) and (20).

$$\begin{aligned} V_{d,mpp} &= V_{mpp} + I_{mpp}R_s \\ &= V_{mpp} + I_{mpp}R_{add} - I_m R_s \end{aligned} \tag{22}$$

where R_{add} is the additional series resistance, $V_{d,mpp}$ is the equivalent diode voltage at the MPP, and V_{mpp} and I_{mpp} are the output voltage and current, respectively. The expression of R_{add} can be obtained by (22).

$$R_{add} = \frac{I_{mpp} + I_m}{I_{mpp}} R_s = \frac{I_{sc}}{I_{mpp}} R_s \simeq R_s \tag{23}$$

where I_{sc} is the short-circuit current of the PV module, which is the same value of I_{ext}. From (23), the additional series resistance which improves the emulation accuracy at the MPP can be obtained. Generally, since the short-circuit current and the MPP current are very similar to each other (because of $I_{mpp}>>I_m$), R_{add} can be approximated to R_s as shown in Fig. 4.7. This is the same approximation as shown in (21). Therefore, the additional series resistance can be selected to be equal to the equivalent series resistance R_s or to be slightly higher than R_s by multiplying R_s and the ratio of short-circuit current to the MPP current as shown in (23).

The proposed emulation method can improve the accuracy at the MPP by simply adding the series

ULSAN NATIONAL INSTITUTE OF SCIENCE AND TECHNOLOGY

resistor without additional equipment, control algorithms and active devices. The PV module of DPP system operates at the MPP. Therefore, the PV emulator accuracy at the MPP is significant in its applications. When the conventional PV emulator is used to test the DPP system, the voltage of the PV module is increased. It changes the nominal operating point of the power converter. Since the DPP converter is designed to the characteristics of the real module, it does not accurately confirm the performance when the converter is applied to the actual installation environment. In addition, when it is optimally designed and the design margin is low, there is a risk that the device inside the circuit fails due to the increased voltage. On the other hand, using the proposed method, the accuracy at the MPP is compensated, then the DPP converter operates at the desired operating point. This is because each PV module operates at the MPP in the DPP system. Therefore, the performance of the DPP system can be accurately confirmed with the proposed emulation method.

4.3 Experimental Verifications

This section experimentally demonstrates the performance and accuracy of the proposed PV emulation method operating at the MPP. The proposed emulation method is verified by the measurement data of the outdoor experiments and the conventional emulation method with MPP operations, and *P-V* and *I-V* characteristic curves. SCM40W PV modules manufactured by Solarcenter are used in this experiment. The parameter of the PV modules and additional resistance for the error compensation are listed in Table IV.

Fig. 4.8 shows the experimental set-up of the outdoor experiment and the indoor PV emulation. The outdoor experiment has difficulties in installing and is affected by external environments. Compared with the outdoor experiment, the indoor PV emulation experiment can be easily conducted with stable circumstances.

Fig. 4.9 shows the *I-V* and *P-V* characteristic curves of the outdoor experiment, the conventional emulation method, and the proposed emulation method. Experiments have been conducted according to the irradiance conditions of 610, 800, and 1090 W/m^2, respectively. It shows that the proposed PV emulation method can provide higher accuracy at the MPP than that of the conventional one. Besides, the accuracy at the MPP can be enhanced regardless of the change in the amount of irradiance.

The MPPs of the sunlight, the conventional method, and the proposed method are listed in Table II. The MPP of the conventional emulation method has higher voltage than that of the MPP of the sunlight. It causes the accuracy reduction of the PV output voltage emulation. As a result, the conventional method has MPP power errors of 6.18%, 10.36%, and 12.75% for 610 W/m^2, 800 W/m^2, and 1090 W/m^2, respectively. On the other hand, the proposed emulation method has similar MPPs comparing with the real sunlight cases because the accuracy of the MPP is compensated by the additional series resistor. In particular, the accuracy in the MPP is greatly compensated, which shows that the proposed emulation

ULSAN NATIONAL INSTITUTE OF SCIENCE AND TECHNOLOGY

TABLE IV EXPERIMENTAL SET-UP PARAMETERS

Parameter	Mark	Value
Maximum Power	P_{mpp}	40 [W]
Voltage at MPP	V_{mpp}	19.5 [V]
Current at MPP	I_{mpp}	2.18 [A]
Open-Circuit Voltage	V_{oc}	23.6 [V]
Short-Circuit Current	I_{sc}	2.30 [A]
Additional Resister	R_{add}	1.2 [Ω]

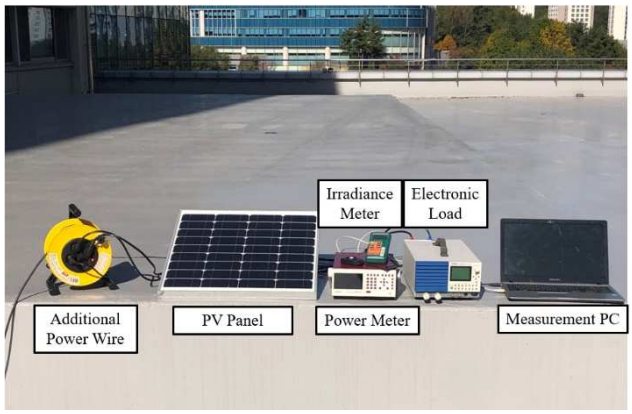

(a) Outdoor experiment

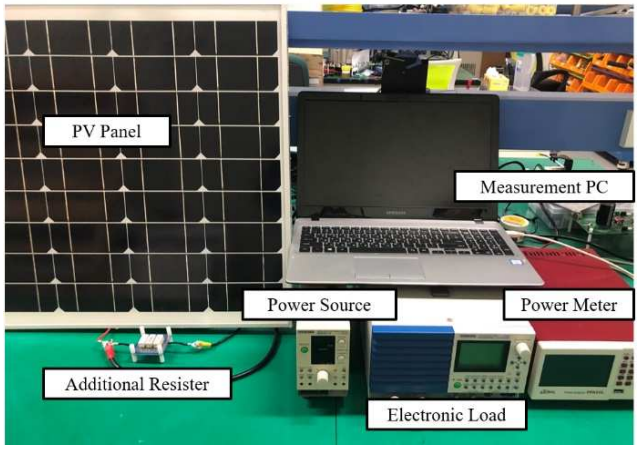

(b) Indoor PV module emulation

Fig. 4.8. Photographs of the experimental set-up

method has MPP power errors of 0.63%, 0.88%, and 0.34% for 610 W/m^2, 800 W/m^2, and 1090 W/m^2, respectively. As a result, the proposed PV emulation method compensates the MPP error to improve the emulation accuracy, which is experimentally verified.

The overall errors between the real *I-V* characteristic curves and the emulated *I-V* characteristic curves are summarized in Table VI, where the errors are calculated using the mean relative error (MRE) criterion.

ULSAN NATIONAL INSTITUTE OF
SCIENCE AND TECHNOLOGY

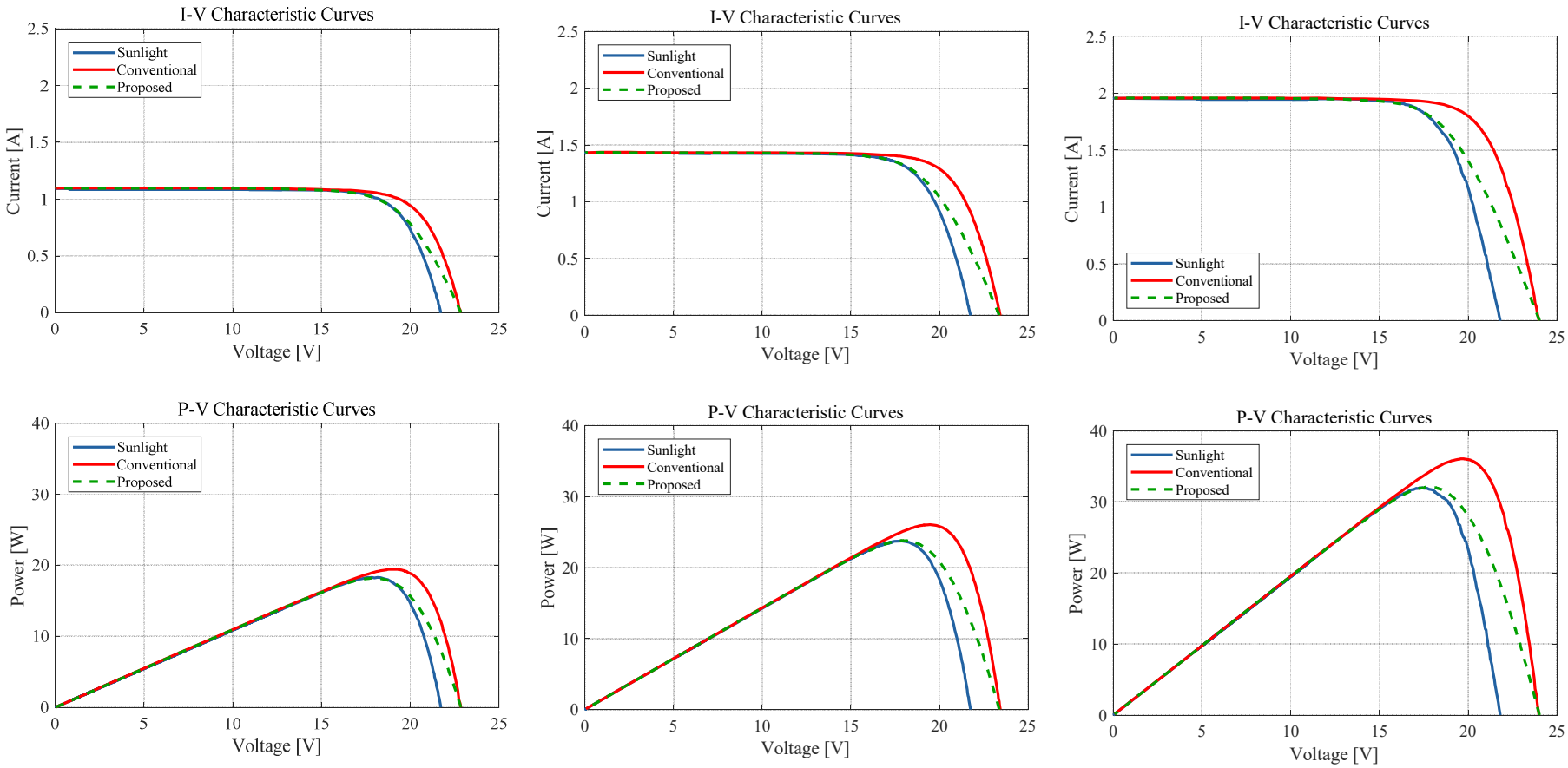

(a) 610 W/m^2 (b) 800 W/m^2 (c) 1090 W/m^2

Fig. 4.9. Experimental *I-V* and *P-V* characteristic curve results at three irradiance levels

ULSAN NATIONAL INSTITUTE OF SCIENCE AND TECHNOLOGY

TABLE V COMPARISON OF OPERATING PARAMETERS AT MPP

Irradiance [W/m^2]	Method	V_{mpp} [V]	I_{mpp} [A]	P_{mpp} [W]	P_{mpp} Error [%]
610	Sunlight	17.85	1.026	18.31	-
	Conventional	18.88	1.030	19.45	6.18
	Proposed	18.09	1.006	18.20	0.63
800	Sunlight	17.31	1.363	23.59	-
	Conventional	19.46	1.338	26.04	10.36
	Proposed	17.87	1.332	23.80	0.88
1090	Sunlight	17.27	1.853	32.00	-
	Conventional	19.63	1.838	36.08	12.75
	Proposed	17.80	1.804	32.11	0.34

TABLE VI MRE BETWEEN SUNLIGHT AND EMULATION OF THE *I-V* CURVE

Irradiance [W/m^2]	MRE of the conventional method	MRE of the proposed method
610	4.99%	2.15%
800	7.34%	3.26%
1090	9.85%	4.69%

The MREs of the conventional method are 4.99%, 7.34%, and 9.85% for 610 W/m^2, 800 W/m^2, and 1090 W/m^2, respectively. Using the proposed method, the MREs of the emulation decrease to 2.15%, 3.26%, and 4.69%. Using the MRE analysis, it is verified that the accuracy of the overall PV characteristic curves is also improved.

As, a result, the proposed PV emulation method is verified the improved accuracy compared with the outdoor experiments and the conventional emulation method. The power error of the proposed emulation method at the MPP is smaller than that of the conventional emulation method. It is confirmed that the MPP power errors of 5.55%, 9.48%, and 12.41% for each irradiance are compensated compared to the conventional emulation methods. In addition, it is confirmed that the overall PV characteristic curve MRE is compensated by 2.84%, 4.08%, and 5.16% for each irradiance compared to the conventional method.

ULSAN NATIONAL INSTITUTE OF SCIENCE AND TECHNOLOGY

4.4 DPP Operations under Various Shading Conditions

The experiment of the DPP system was performed out using the indoor PV emulator proposed in chapter 5. Fig. 4.10 shows the experimental setup of the DPP system. The flyback converter used in the experiment was constructed using the design methodology presented in chapter 3 and the parameters are listed in Table III. The PV module is made of blue coated glass on the outside for building integrated photovoltaic (BIPV). The parameters of the PV modules are listed in Table VII. The experimental setup consists of power supplies, PV modules, an oscilloscope, flyback converters, power meters, an electronic load, and a PV inverter.

Fig. 4.12 shows experimental verification of in-lab emulation for DPP. The partial shading condition setup and experimental results for this verification are summarized in Table VIII. In the condition of 50% shade of PV 1, the power generation of DPP system in real sunlight is compared with the power generation of DPP system of the proposed emulation method. The DPP system average power for 300 seconds in real sunlight is 191.85 W and The DPP system average power of the proposed emulation method is 190.61 W. The results of these two experiments have almost the same value, and the power generation error of the emulation method is about 0.13%. Therefore, it is verified that the proposed emulation method has high accuracy and is suitable for DPP system performance test. DPP system performance experiments are conducted using the proposed in-laboratory emulation method. This allows experiments with various shading conditions under stable conditions.

The performance experiments of the DPP system consists of experiments of measuring PV-characteristic curves and experiments measuring the power for 600 seconds in conjunction with a PV inverter. Each experiment confirms and compares the results of a serial connection system and a DPP system various partial shading conditions. There are six shading conditions. Table VIIII shows the solar irradiance conditions for each case. The experimental results are shown in Table X and Fig. 4.12. Table X lists the maximum power of the *P-V* characteristic curve and the PV inverter interlock average power.

Fig. 4.12 shows the *P-V* characteristics curve and the PV inverter interlocking output power by various shading case. As shown in the experimental results, in case 1 where all panels have the same

TABLE VII EXPERIMENTAL PV MODULE PARAMETERS

Parameter	Mark	Value
Maximum Power	P_{mpp}	63 [W]
Voltage at MPP	V_{mpp}	15.28 [V]
Current at MPP	I_{mpp}	4.13 [A]
Open-Circuit Voltage	V_{oc}	18.35 [V]
Short-Circuit Current	I_{sc}	4.40 [A]

ULSAN NATIONAL INSTITUTE OF
SCIENCE AND TECHNOLOGY

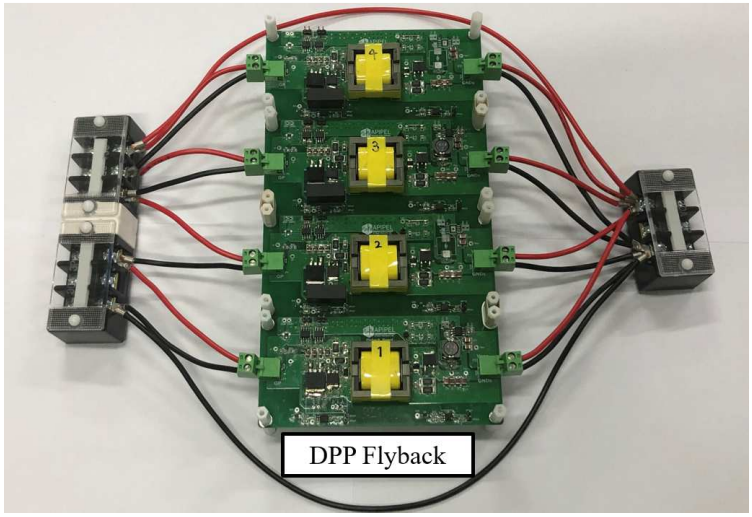

(a) Bidirectional flyback converter for DPP system

(b) PV modules

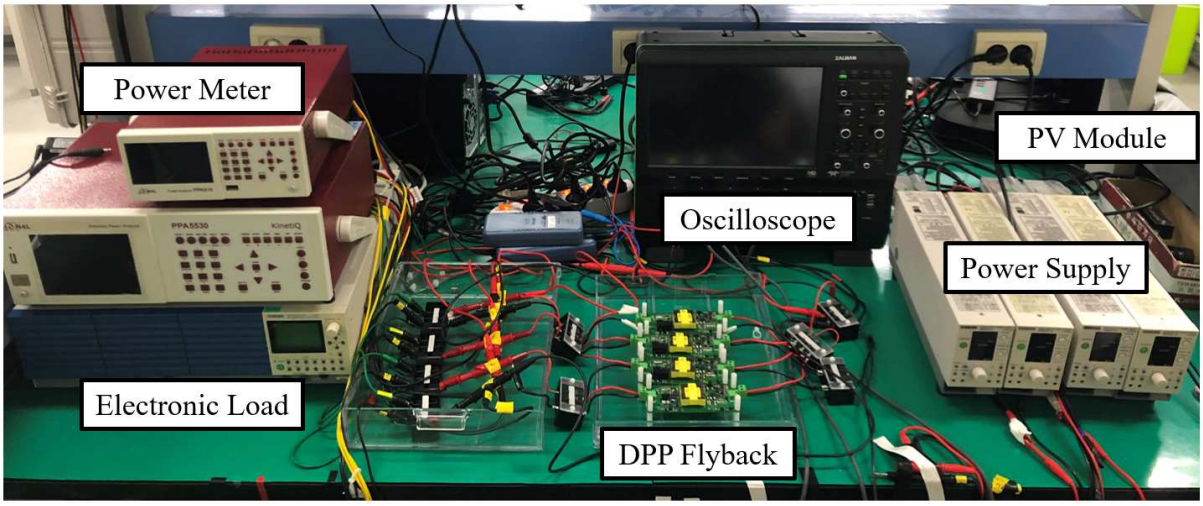

(c) DPP experimental setup

Fig. 4.10. Photographs of DPP experimental system

ULSAN NATIONAL INSTITUTE OF SCIENCE AND TECHNOLOGY

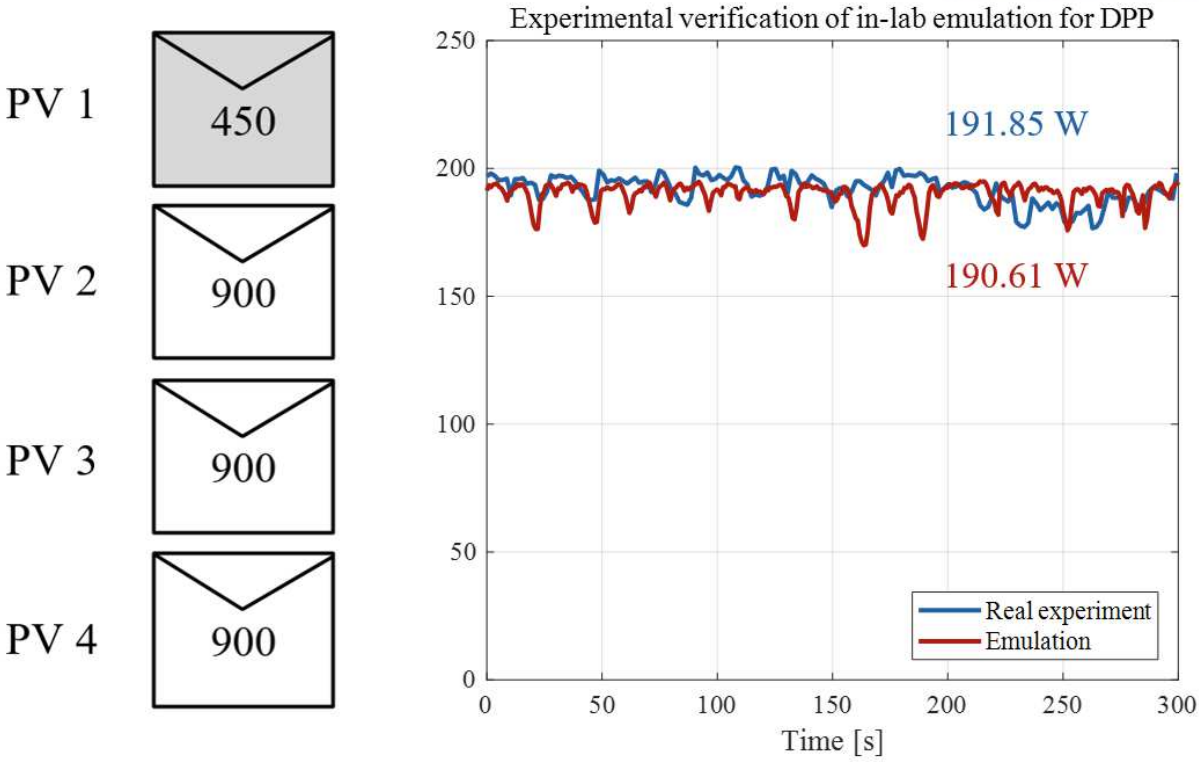

(a) Irradiance condition (b) Power comparison experiment and emulation for DPP

Fig. 4.11. Experimental verification of in-lab emulation for DPP

TABLE VIII EXPERIMENTAL SETUP AND RESULTS OF IN-LAB EMULATION FOR DPP

PV 1	PV 2	PV 3	PV 4	Real power	Emulation power	Power error
450 W/m^2	900 W/m^2	900 W/m^2	900 W/m^2	191.85 W	190.61 W	0.13 %

amount of solar irradiance, the generation power of the series connection system is higher than that of the DPP system. It is because it includes gate driver drive losses, sensor losses, and flyback converter losses to drive the DPP system. In all other uneven shading cases except case 1, it can be seen that the generated power of the DPP system is higher than that of the series connection system. Cases 4 and 6 show the highest difference between the maximum power of the series system and the DPP system at 129% and 137%. As shown in the PV inverter interlock experimental results, the PV inverter used in the experiment does not have global MPP operation. Therefore, the power of the series connection system operates at the local MPP with the highest voltage. This makes the power generation difference between the DPP system and the series connection system larger in the PV inverter interlocking experiment than in the *P-V* verification experiment. Since the DPP system performs MPPT simultaneously in the DPP converter and the PV inverter, it can be seen that the power fluctuation is

ULSAN NATIONAL INSTITUTE OF SCIENCE AND TECHNOLOGY

TABLE VIIII IRRADIENCE OF PV MODULES BY VARIOUS SHADING CASES

	Case 1	Case 2	Case 3	Case 4	Case 5	Case6
PV 1	900 W/m^2	675 W/m^2	450 W/m^2	450 W/m^2	450 W/m^2	225 W/m^2
PV 2	900 W/m^2	900 W/m^2	900 W/m^2	450 W/m^2	450 W/m^2	450 W/m^2
PV 3	900 W/m^2	900 W/m^2	900 W/m^2	900 W/m^2	450 W/m^2	675 W/m^2
PV 4	900 W/m^2	900 W/m^2	900 W/m^2	900 W/m^2	900 W/m^2	900 W/m^2

TABLE X EXPERIMENTAL RESULT BY VARIOUS SHADING CASES

Experiment	System	Case 1	Case 2	Case 3	Case 4	Case 5	Case6
Maximum power of the *P-V* characteristic curve	Series	237.81 W	197.36 W	172.61 W	129.24 W	121.89 W	95.91 W
	DPP	232.89 W	216.58 W	198.39 W	167.12 W	131.87 W	131.84 W
	DPP ratio to series	97.93%	109.74%	114.94%	129.31%	108.19%	137.46%
PV inverter interlock average power	Series	232.05 W	191.99 W	131.84 W	125.16 W	118.24 W	63.61 W
	DPP	223.91 W	207.63 W	190.44 W	159.87 W	127.63 W	127.83 W
	DPP ratio to series	96.49%	108.15%	144.45%	127.73%	107.94%	200.96%

larger than the series connection system. At present, the MPPT cycle of PV inverter is about 167ms and the MPPT cycle of DPP converter is about 8ms set to be about 20 times by operating at about 8ms, so it is set to have a difference of about 20 times.

It was confirmed that the DPP system produces higher power than the series connection system in all shade conditions except the even condition. The largest difference in MPP power is about 37% and the largest inverter interlocking power difference is about 100.96%. As a result, the effectiveness of DPP system and power control algorithm was verified.

ULSAN NATIONAL INSTITUTE OF SCIENCE AND TECHNOLOGY

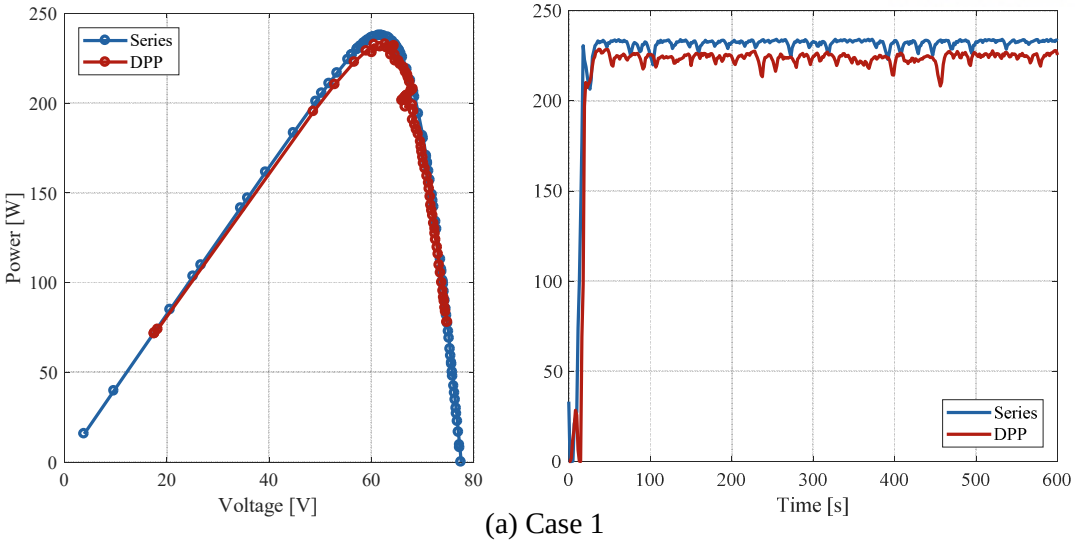

(a) Case 1

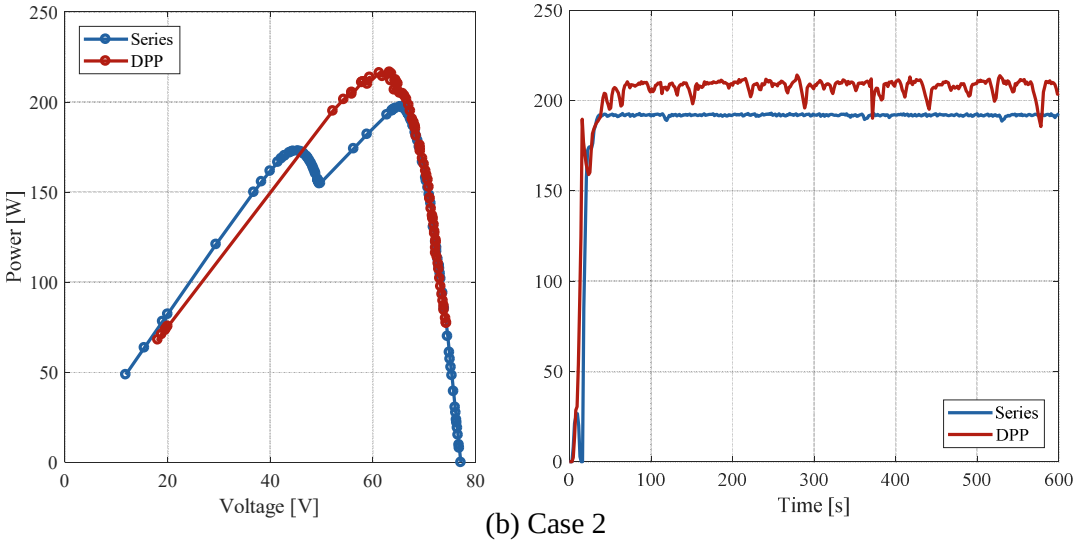

(b) Case 2

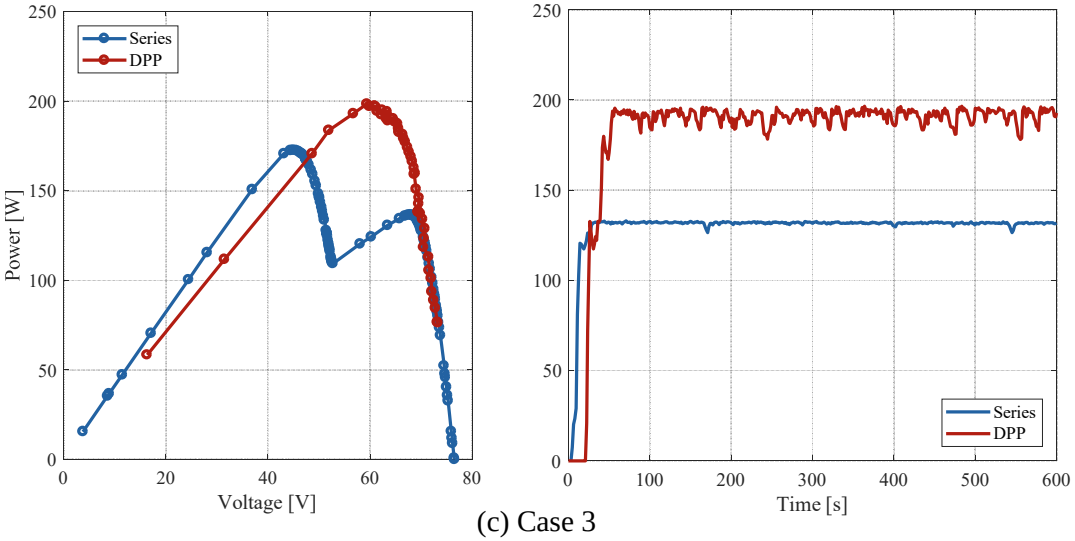

(c) Case 3

ULSAN NATIONAL INSTITUTE OF
SCIENCE AND TECHNOLOGY

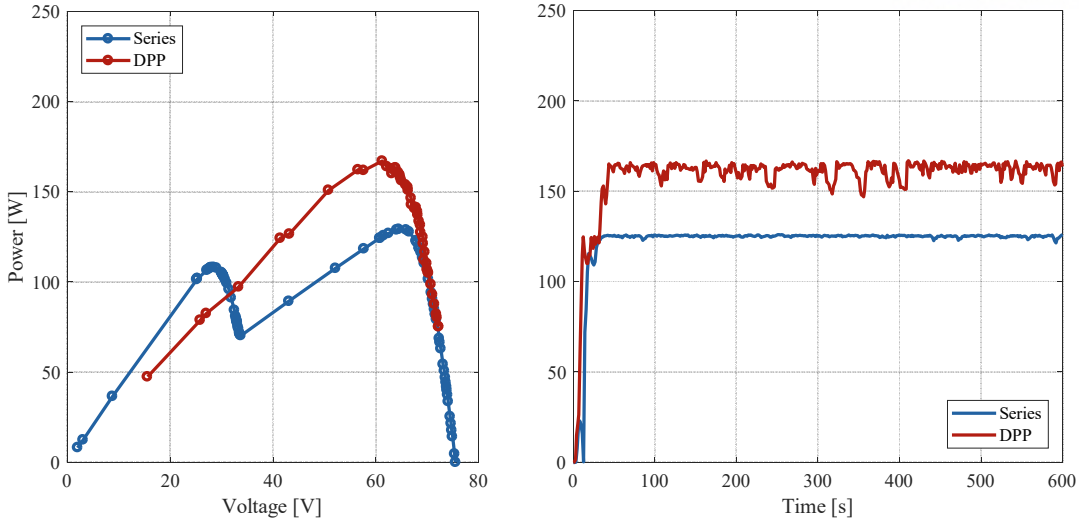

(d) Case 4

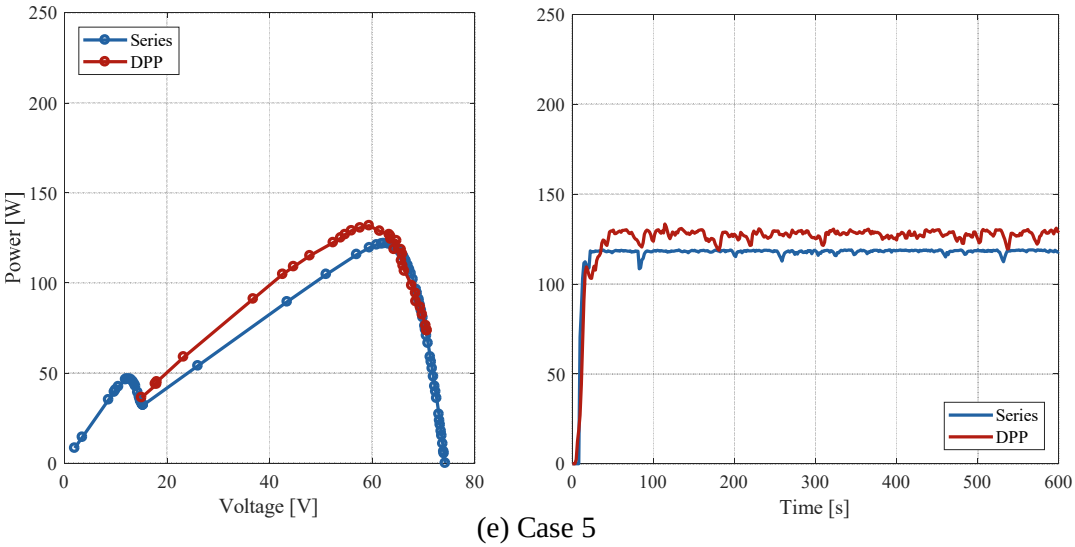

(e) Case 5

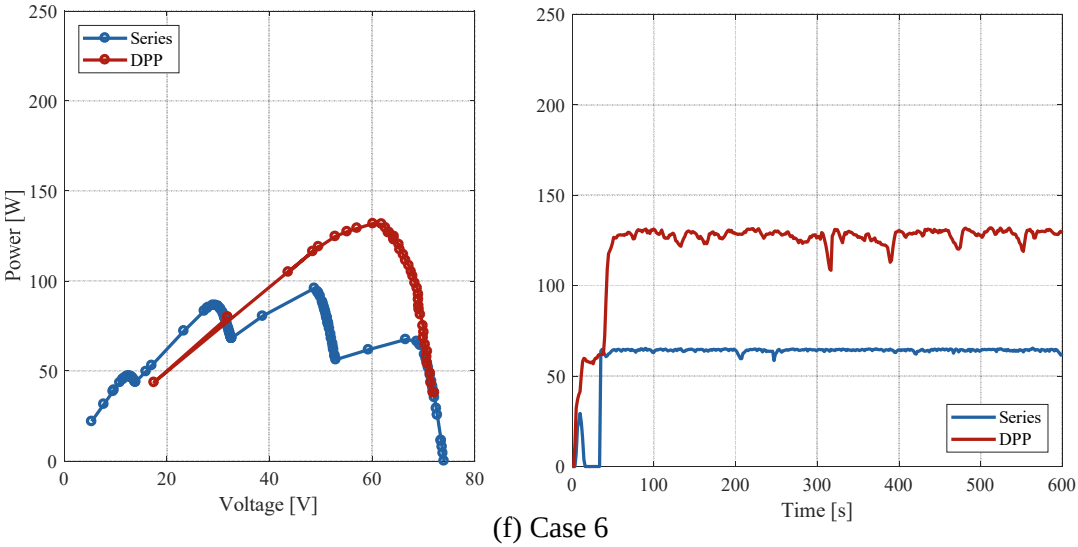

(f) Case 6

Fig. 4.12. P-V characteristics curve and PV inverter interlocking output power by various shading case

ULSAN NATIONAL INSTITUTE OF
SCIENCE AND TECHNOLOGY

V. Protection Algorithm Development of DPP using PHIL Simulations

In a DPP system, a differential converter is configured in parallel to the PV module for MPP operation. It makes the system less reliable than a PV series connection system. Because of the risk of failure, this is less reliable than a series connection system without other failure components. In the DPP architecture diagram in Figure 1.2, if the DPP converter continues switching operation because the converter is not aware of the short-circuit failure situation, it can lead to fatal hazard. Therefore, DPP system needs a protection algorithm to cope with low reliability. This thesis develops a protection algorithm to improve the reliability of the DPP system and verify the protection algorithm developed by modeling the DPP system and failure conditions through power hardware-in-the-loop (PHIL) simulation.

5.1 Concept of the PHIL Simulations

Hardware-in-the-loop (HIL) simulation is a type of real-time simulation. It is a verification method that performs real-time simulation by modeling a plant to verify a real algorithm or controller. The PHIL simulation is a HIL simulation that includes power equipment with power interface and hardware under test (HUT) as shown in Fig. 5.1. That is, part of the power plant consists of real hardware, and the real controller controls both the real hardware and the plant inside the real-time simulator. It is possible to check not only the actual controller but also the power converter composed of hardware in real time. This thesis uses PHIL simulation to test the failure conditions of DPP systems that are difficult to implement in practice. For this purpose, PV modules, DPP differential converters, PV inverters and fault conditions are modeled. One differential converter in a DPP system plant consists of real hardware. It verifies the steady state operation of the DPP system and the operation of the protection algorithm developed in case of failure and the differential converter operation accordingly. Through this, developed DPP system protection algorithm is verified.

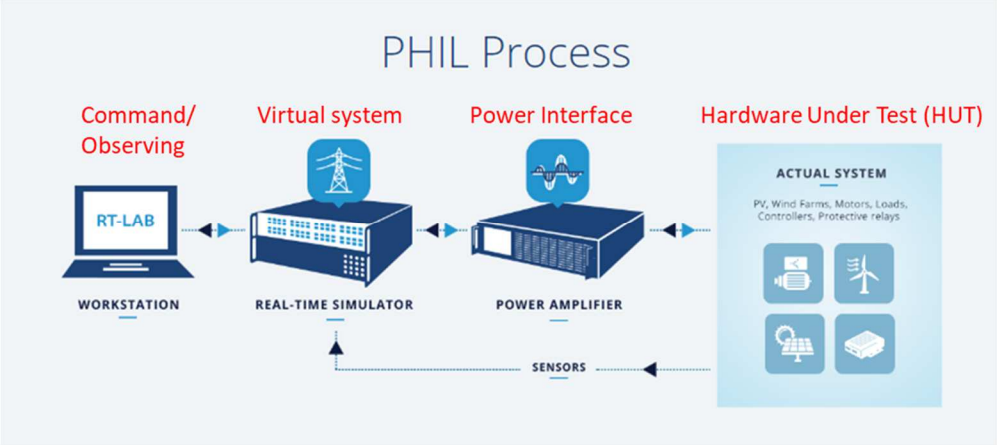

Fig. 5.1. Concept of the PHIL simulation [27]

ULSAN NATIONAL INSTITUTE OF
SCIENCE AND TECHNOLOGY

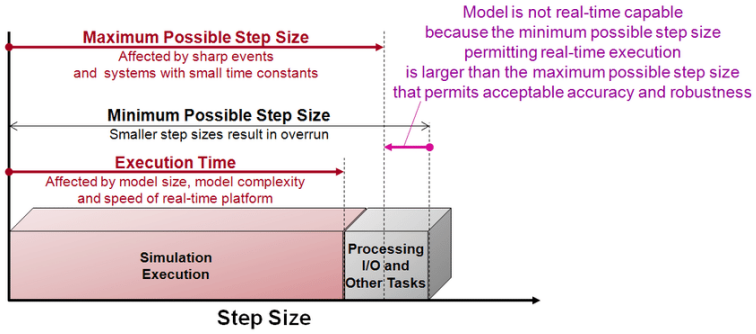

Fig. 5.2. Step size calculation of the PHIL simulation [27]

5.2 Configuration of Real-time DPP Model

5.2.1 Real-time Simulation Target Performance

To enable real-time simulation, the model calculations must be performed in the simulator within the specified time step as show in Fig. 5.2. If the model calculation time is longer than this time step, an overrun occurs and real-time simulation is not possible. Therefore, it is necessary to check the accuracy of the model and the model calculation time to select the appropriate level for the real-time simulation operation. Since the implemented DPP system controller operates at 20μs period, the time step of the real-time simulation model is also selected as 20μs. The real-time simulator used OP5600 machine of the opal-rt. Target accuracy of PV modules and DPP differential converters is modeled to be over 90% accurate with real systems.

5.2.2 PV Model

Because the model must be calculated within the time step for real-time simulation, the proper distribution of model accuracy and computation time is important. The dynamic PV model in Fig. 5.3 is the most accurate PV model that can calculate all internal parameters, including solar radiation, temperature, and internal current changes. However, this requires high computational burden because of its high accuracy but requires Numerical Iteration. Since the OP5600 supports the Matlab Simulink-based platform, the PV model based on the five parameter model provided by Matlab Simulink can be used as shown in Fig. 5.4. This model has a relatively low accuracy but requires only a low computational burden. The final PV model to be introduced is the lookup table model as shown in Fig. 5.5. This is the model used in typical PV emulators. The high-accuracy model has high accuracy because it extracts and uses output current data of various operating situations. Based on the data, the accuracy is lowered when operating on the data other than the input data. Since there is no Numerical Iteration,

ULSAN NATIONAL INSTITUTE OF SCIENCE AND TECHNOLOGY

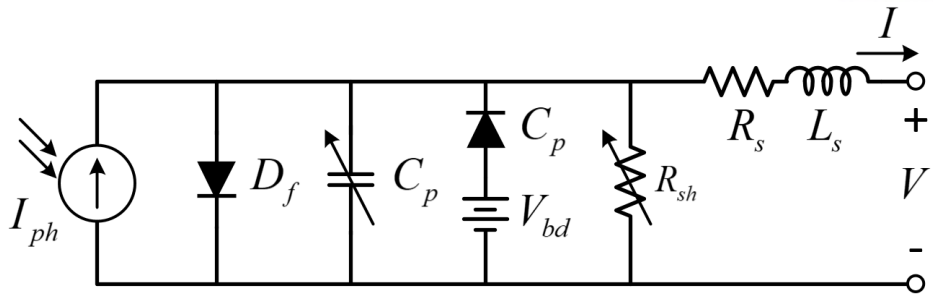

Fig. 5.3. Dynamic PV model [28]

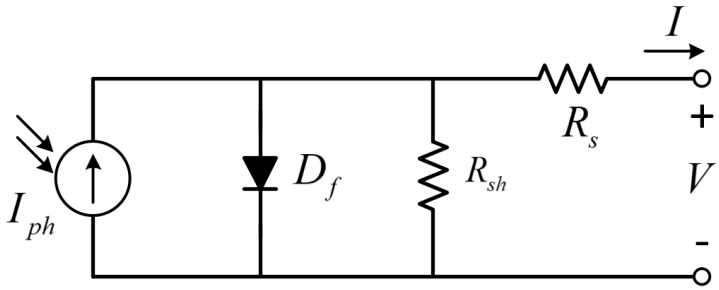

Fig. 5.4. Five-parameters PV model

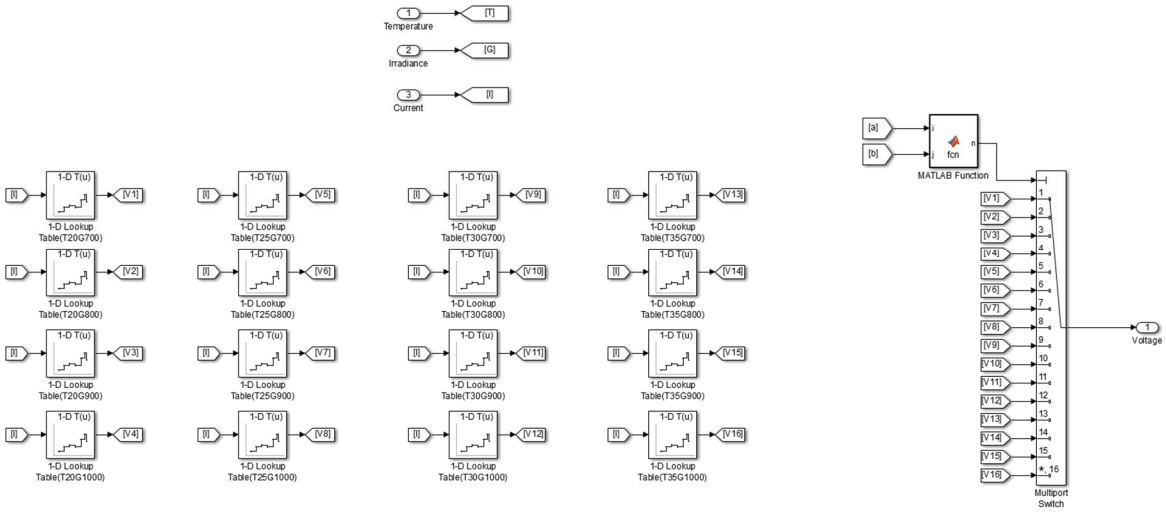

Fig. 5.5. Lookup Table PV model

it has a low computational burden. From these three PV models, the PV model to be used for real-time simulation will be selected considering the model's accuracy and computational burden. Fig. 5.6 shows the *I-V* curve comparison between PV models. In the forward bias region, all three models have similar accuracy. However, the MATLAB model has a large error in the reverse bias region because the breakdown voltage of the internal diode is not emulated. Table XI summarizes the comparison between each PV model. The error of each model represents the accuracy error with the dynamic model with the highest accuracy. As can be seen from the table, the errors in MPP at standard test condition (STC), the

ULSAN NATIONAL INSTITUTE OF SCIENCE AND TECHNOLOGY

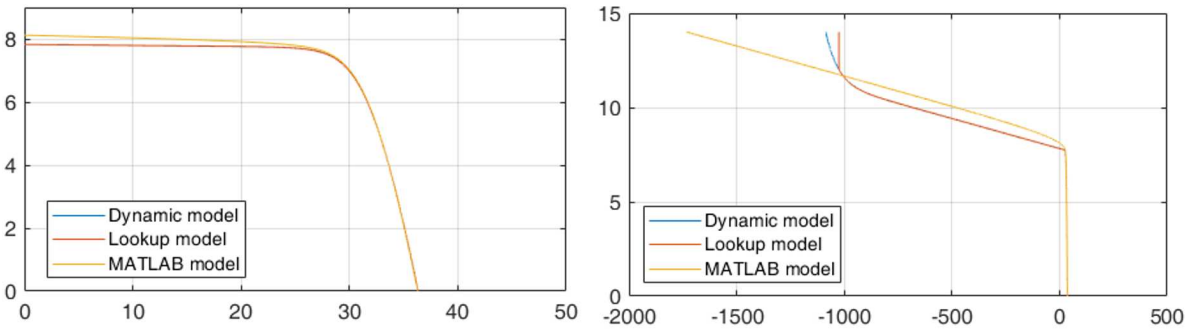

(a) Forward bias region (b) Backward bias region

Fig. 5.6. *I-V* curve comparison between PV models

TABLE XI COMPARISON BETWEEN PV MODELS

	Dynamic PV model	MATLAB PV model	Lookup Table PV model
STC V_{mpp} error	-	0.672%	0.068%
STC I_{mpp} error	-	0.025%	0.055%
STC P_{mpp} error	-	0.698%	0.123%
STC *MRE* error	-	27.33%	1.02%
Average calculation time per panel	6.5 μs	0.2 μs	0.23 μs
Average calculation time for 4 panel	47.61 μs	0.5413 μs	0.6647 μs

forward bias region are all very low, less than 1%. However, in the MRE error comparing the entire curve, the MABLAB model has a large error of 27.33% because of the large error in the reverse bias. On the other hand, the lookup table model has a low error of about 1%. The average calculation time of the four panels of the dynamic PV model is about 47.61μs, which cannot be used for real-time simulation of DPP systems beyond the simulation time step of 20μs. On the other hand, the MATLAB model and lookup table model have a low computation time of about 0.2μs and can be used for real-time simulation of DPP systems. In conclusion, a look-up table PV model with high accuracy and low model calculation was selected as the real-time simulation PV model of the DPP system.

5.2.3 Bidirectional Flyback Converter Model

As with the PV model, the real-time simulation of the DPP system also considers the computation time of the flyback converter, a DPP differential converter. Power conversion circuits such as flyback

ULSAN NATIONAL INSTITUTE OF SCIENCE AND TECHNOLOGY

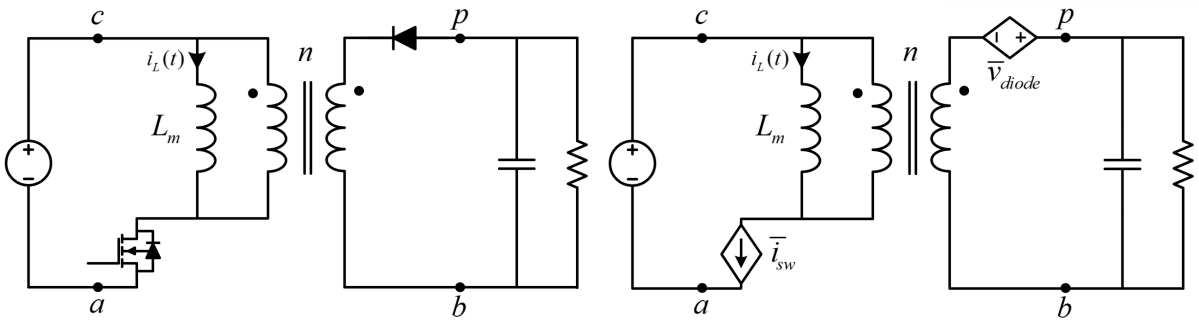

(a) Switching model (b) Average model

Fig. 5.7. Unidirectional flyback converter averaging modeling [29]

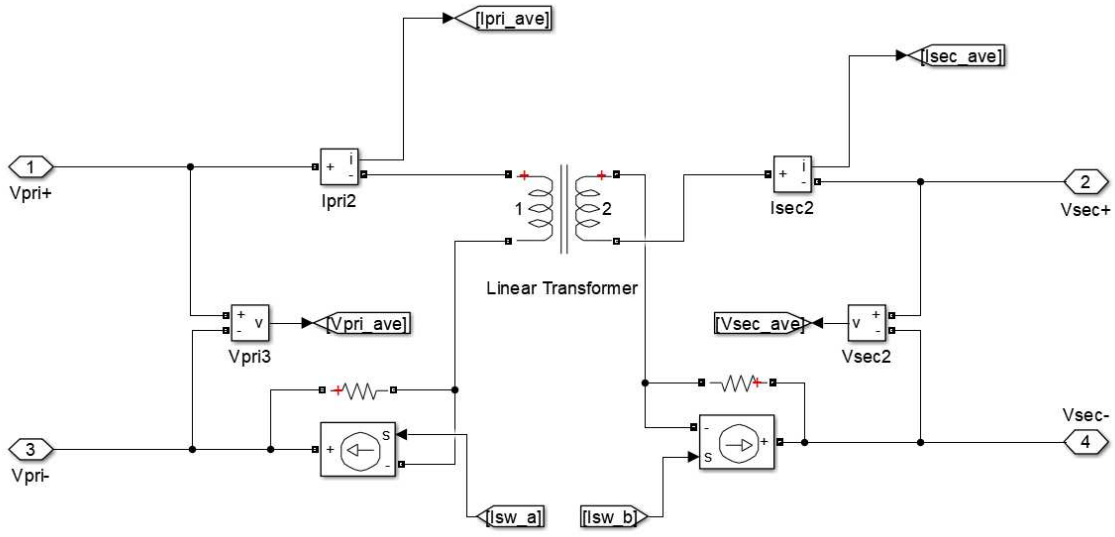

Fig. 5.8. Averaging model of bidirectional flyback converter

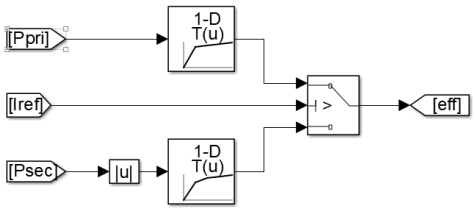

Fig. 5.9. Power conversion efficiency Look-up Table block

converters basically consist of a switching model. However, the switching model requires a high computation burden because the circuit is converted according to the switching operation. Therefore, average modeling is performed to perform the same steady-state operation and to reduce computation time. Fig. 5.7 shows the average modeling of a unidirectional flyback converter [29]. Unidirectional flyback converters can be modeled in an average model by changing diodes and switches to dependent

ULSAN NATIONAL INSTITUTE OF SCIENCE AND TECHNOLOGY

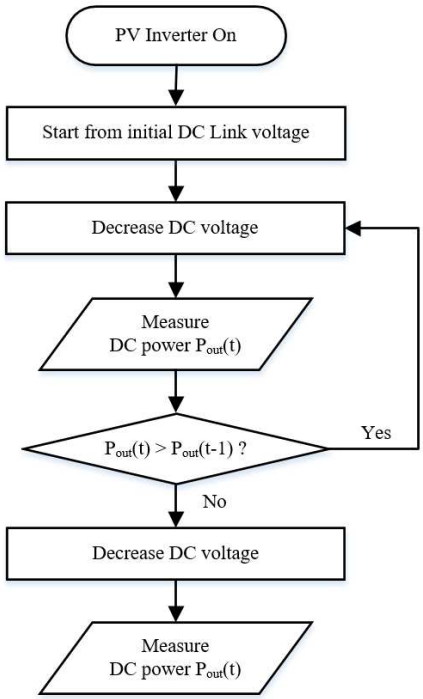

Fig. 5.10. P&O algorithm of PV inverter

voltage and current sources. Since the flyback converter of the implemented DPP system is designed in DCM, average modeling is performed in DCM domain. The unidirectional flyback converter in the DCM domain is averaged modeled by equations (13) and (14).

$$\bar{i}_{sw} = \frac{d_1 i_L}{d_1 + d_2} \tag{13}$$

$$\bar{v}_{diode} = (1-d_2)\bar{v}_{pb} - d_1 n \bar{v}_{cb} \tag{14}$$

where d_1 is the duty ratio, d_2 is the duty ratio, i_L is the magnetization current, and n is the transformer turn ratio.

Similarly, bidirectional flyback converters enable average modeling by changing both primary and secondary switches to dependent current sources. Fig. 5.8 shows the average model configuration of a bidirectional flyback converter. The value of the dependent current source in DCM is given by the following equations (15) and (16).

$$\bar{i}_{sw\_a} = \frac{{d_1}^2 T V_{pri}}{2L_m},\ \bar{i}_{sw\_b} = -\frac{\eta_{for} V_{pri} I_{pri}}{V_{\sec}} \tag{15}$$

$$\bar{i}_{sw\_a} = -\frac{\eta_{back} V_{\sec} I_{\sec}}{V_{pri}},\ \bar{i}_{sw\_b} = \frac{{d_1}^2 T V_{\sec}}{2L_m n^2} \tag{16}$$

Equation (15) is an average modeling equation in the forward condition, and equation (16) is the average modeling equation in the backward condition. Where η_{for} is the converter power conversion efficiency

ULSAN NATIONAL INSTITUTE OF SCIENCE AND TECHNOLOGY

in the forward condition, η_{back} is the converter power conversion efficiency in the reverse condition, T is the switching period L_m is the magnetizing inductance value.

Bidirectional flyback converter efficiency can be modeled with input and output current magnitudes. The power conversion efficiency confirmed experimentally in Fig. 3.7 was implemented using the lookup table block as shown in Fig. 5.9. Using this method, the bidirectional flyback converter average model that can be used for real-time simulation of DPP systems can be constructed.

5.2.4 PV Inverter Model

The DPP system is connected to a grid-tied PV inverter that performs MPPT as shown in Fig. 2.1. The PV inverter performs the MPPT to enable the operation of the DPP system. In the real-time simulation of the DPP system, a PV inverter model is constructed with P&O algorithm blocks for MPPT. The P&O algorithm flow chart used in the implement the inverter is shown in Fig. 5.10. Since the model is simply composed of algorithm blocks, it does not affect the model calculation time and performs the MPPT function of the PV inverter. Like the PV inverter used in the actual experiment, the MPPT cycle is set to 167ms.

5.2.5 Overall Real-time Simulation Model Configuration for DPP Systems

Fig. 5.11 shows the overall real-time simulation model configuration for DPP systems, which is the component modeled in the previous chapter. The DPP system consists of four PV models, four DPP flyback converter models and an MPPT inverter model. It consists of a block for real-time simulation and a block for communication with a real controller and converter current controller model. The implemented real-time simulation model can operate by itself and PHIL simulation can be performed by replacing part of the implemented system with real power equipment. Fig. 5.12 shows the real-time simulation results of the implemented model. This is the result when the solar irradiance of PV1,2,3 is set to 1000W/m^2 and the solar irradiance of PV4 is set to 500W/m^2. It shows PV inverter operation, PV module voltage and current command of DPP converter, and it is possible to confirm proper operation of DPP system in partial shading of one PV module. The implemented real-time simulation model is used for PHIL simulation to verify the DPP fault protection algorithm.

ULSAN NATIONAL INSTITUTE OF SCIENCE AND TECHNOLOGY

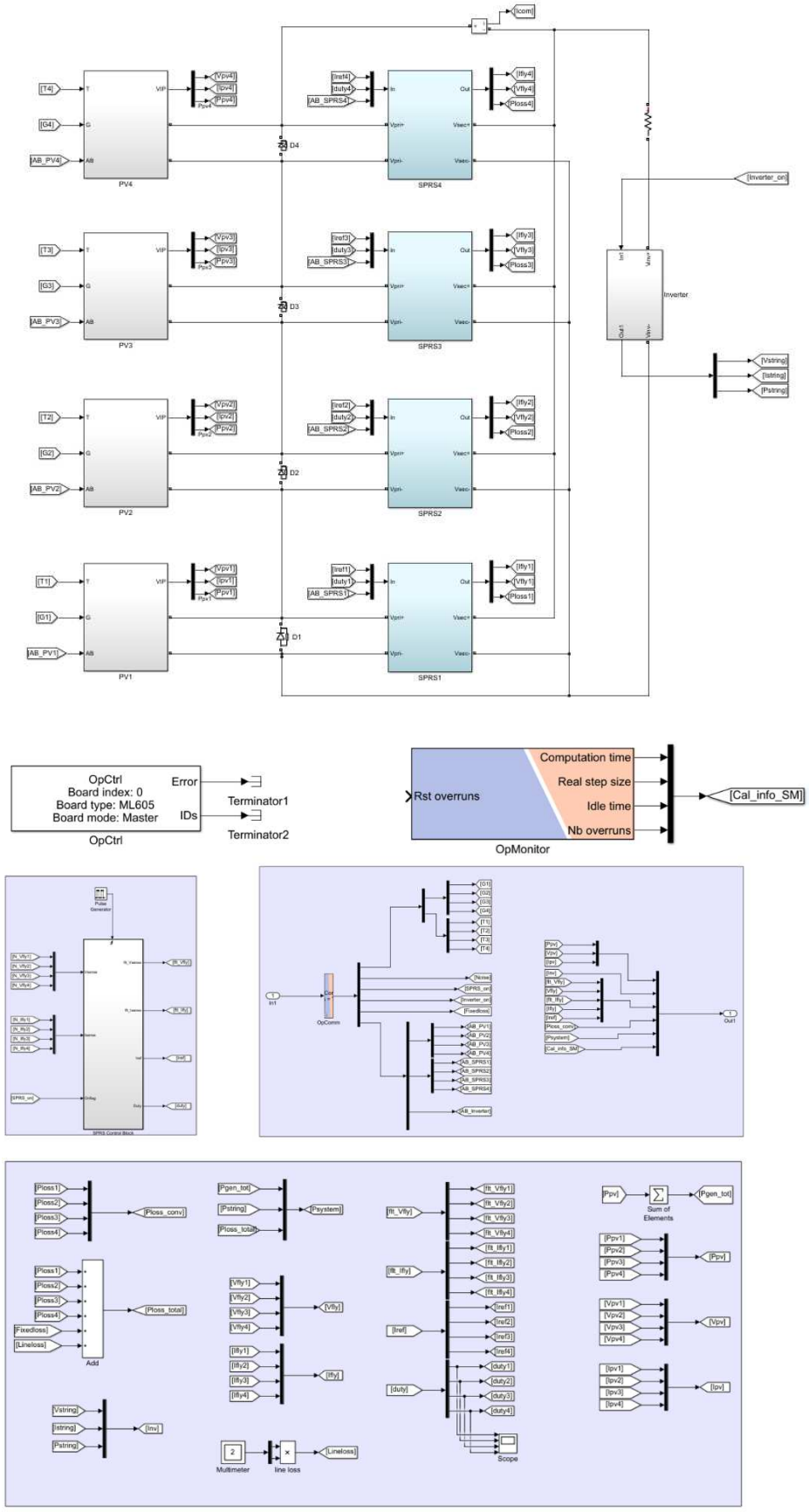

Fig. 5.11. Real-time simulation model configuration for DPP systems

ULSAN NATIONAL INSTITUTE OF SCIENCE AND TECHNOLOGY

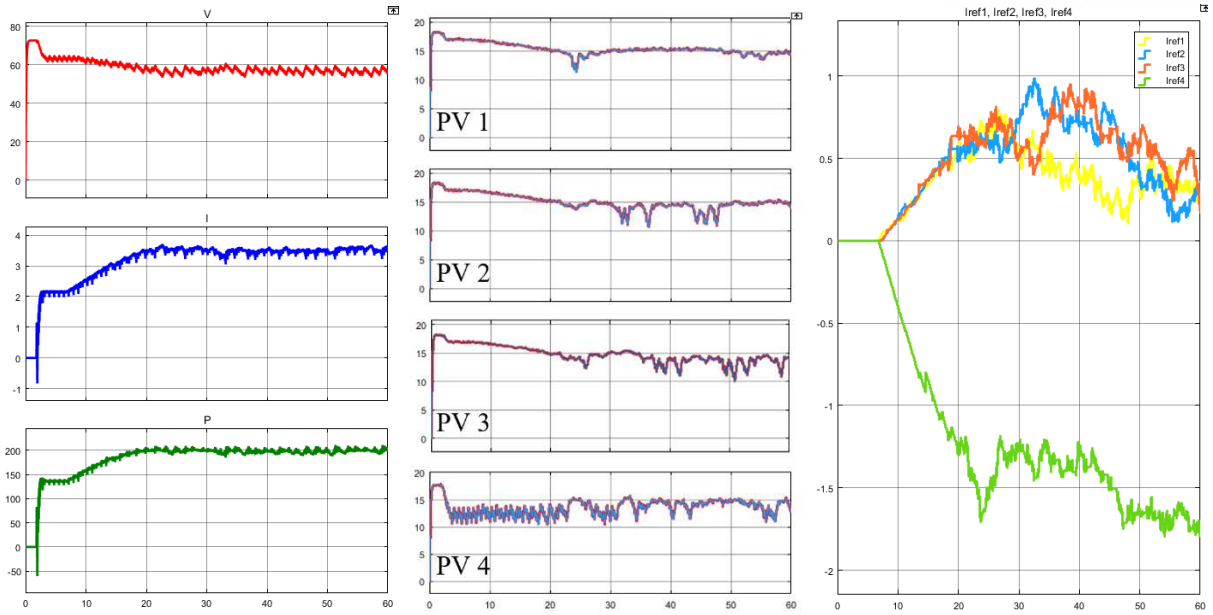

(a) PV inverter operation (b) PV modules voltage (c) Flyback current reference

Fig. 5.12. Real-time simulation operation confirmation

TABLE XII SYMPTOM AND DETECTION BY FAULT CONDITIONS

	PV open	PV short	Primary open	Primary short	Secondary open	Secondary short
DPP converter voltage	0 (correspond PV module)	0 (correspond PV module)	Normal	0 (correspond PV module)	Normal	0 (overall PV module)
DPP converter current	0 (correspond PV module)	High current	0 (correspond PV module)	High current	0 (correspond PV module)	High current
Detection	Low voltage	High current	Current control fails	High current	Current control fails	High current

5.3 Protection Algorithm Development

Since the DPP system is connected in parallel with differential converters, it is more prone to failure than conventional series connection systems consisting solely of PV modules and passive components. Therefore, the development of a corresponding protection algorithm is required. Table XII lists the symptom and detection methods for each fault conditions that can occur in the DPP system. There are six fault conditions: open and short conditions of the PV module, the primary side of the differential converter, and the secondary side of the differential converter. In the case of PV open, the voltage and

ULSAN NATIONAL INSTITUTE OF
SCIENCE AND TECHNOLOGY

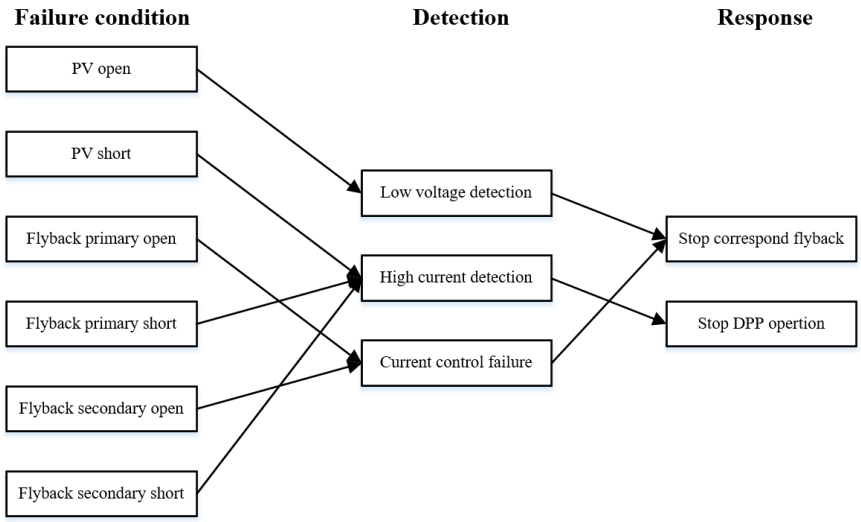

Fig. 5.13. Flowchart of DPP system protection algorithm for each failure condition

current at the input of the DPP converter are recognized as zero. Therefore, a low voltage check is used to detect fault conditions. In the case of PV short, the voltage of DPP converter input is recognized as zero and high current occurs. Therefore, a high current check is used to detect fault conditions. In the case of the flyback converter primary and secondary side open, the voltage is normal, but the current is recognized as zero at the DPP converter input. Therefore, the failure condition is detected by checking the failure of the current control operation. In the case of the flyback converter primary and secondary shorts, a high current is generated at the input of the DPP converter. Therefore, a high current check is used to detect fault conditions. In the case of an open fault situation, the fault condition is solved by stopping the corresponding DPP converter and continuing the generation with the remaining PV. In case of short circuit fault condition, it affects other modules by PV module wiring of DPP system. Therefore, solve the fault condition by stopping the entire DPP system operation. Through this process, the failure situation protection algorithm of the DPP system operates. The flowchart of DPP system protection algorithm for each failure condition is illustrated in Fig. 5.13. The implemented fault protection algorithm will be verified by the PHIL simulation in Chapter VI.

5.4 DPP Protection Algorithm with PHIL Simulations

The simulation of the DPP system protection algorithm verification was performed using the real-time simulation model and protection algorithm developed in chapter 5. Fig. 5.14 shows the PHIL simulation setup for verifying the DPP system fault protection algorithm. The real-time simulation model was modified to replace the number 1 DPP converter model with the actual DPP converter for PHIL operation. The PV module side outputs and DC link side outputs connected to the actual DPP

ULSAN NATIONAL INSTITUTE OF
SCIENCE AND TECHNOLOGY

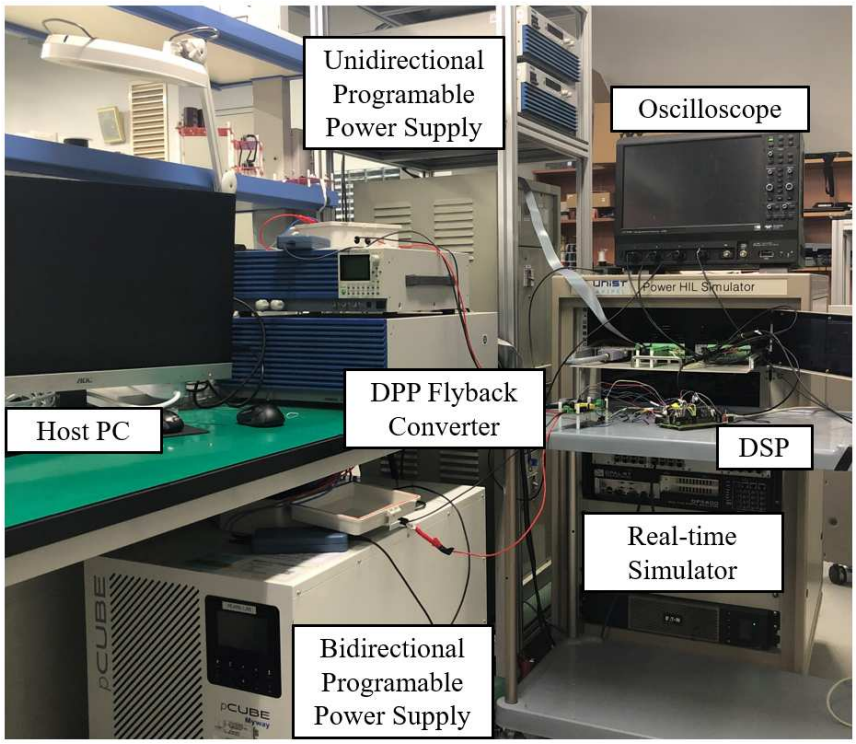

Fig. 5.14. PHIL simulation setup

converter are configured by programmable power supplies. The fault protection algorithm and the DPP power control algorithm are configured in the digital signal processer (DSP). The DSP communicates with the real-time simulator and controls the actual DPP converter and the DPP converter inside the real-time simulation.

Fig 5.15 shows the PHIL simulation result for DPP protection algorithm by fault condition. Each failure situation is summarized in Table XII and implemented as failure of number 1 PV module and converter in PHIL simulation. As the simulation results show, the open fault condition stops the corresponding DPP converter operation and continues power generation to the rest of the DPP system. Short fault conditions stop the entire DPP system and the PV inverter, preventing them from spreading.

In conclusion, the operation of the fault protection algorithm of the DPP system developed using PHIL simulation was verified. The use of protection algorithms verified by PHIL simulation can increase the reliability of the DPP system.

ULSAN NATIONAL INSTITUTE OF SCIENCE AND TECHNOLOGY

(a) PV open fault condition

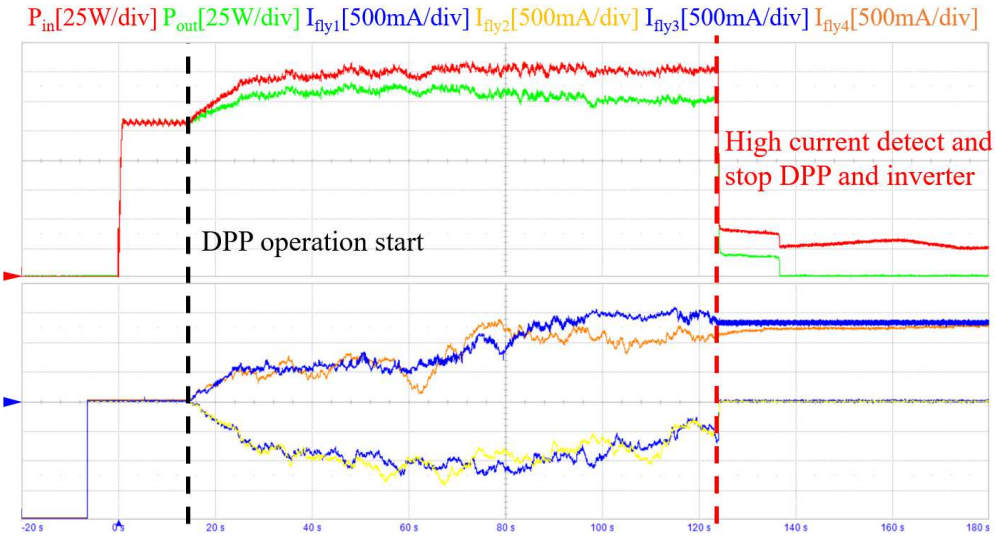

(b) PV short fault condition

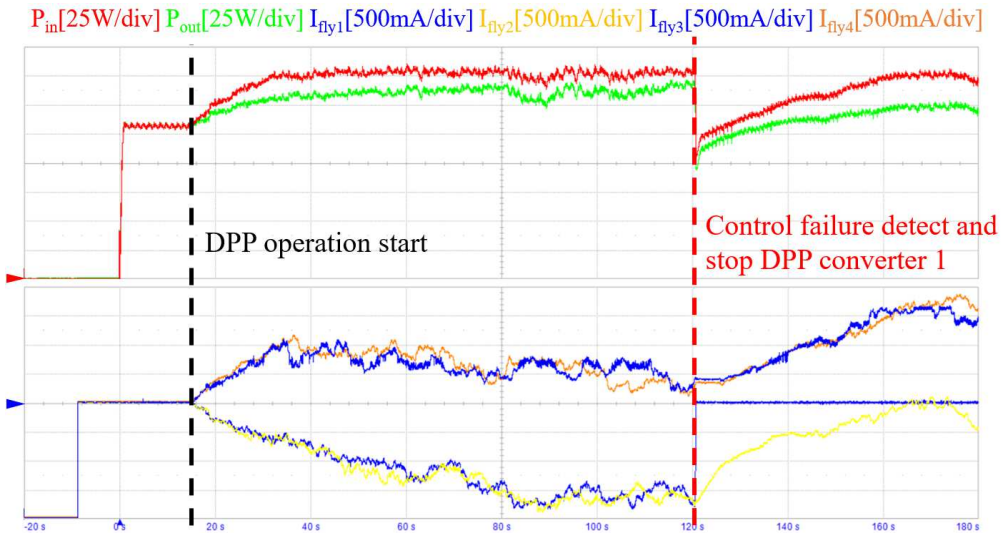

(c) DPP converter primary open fault condition

ULSAN NATIONAL INSTITUTE OF SCIENCE AND TECHNOLOGY

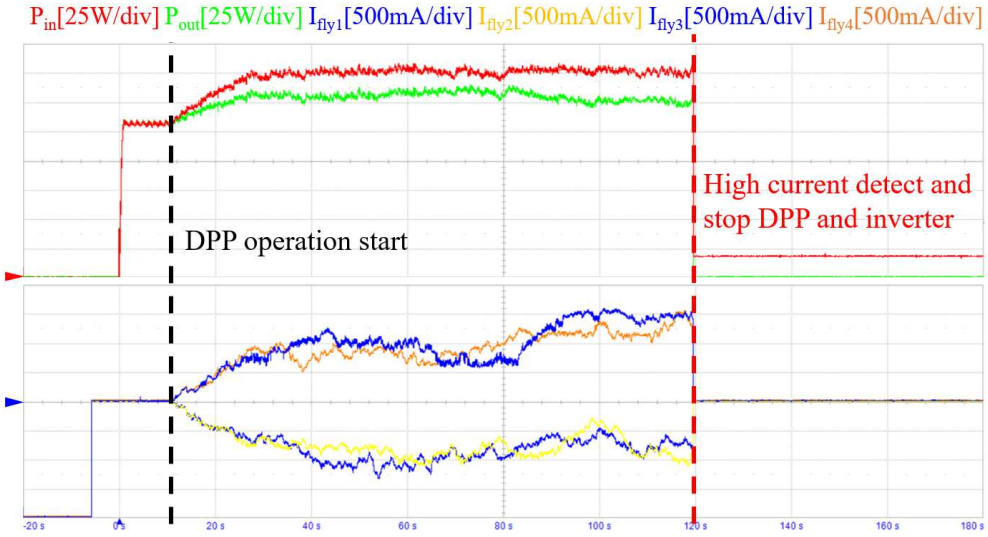

(d) DPP converter primary short fault condition

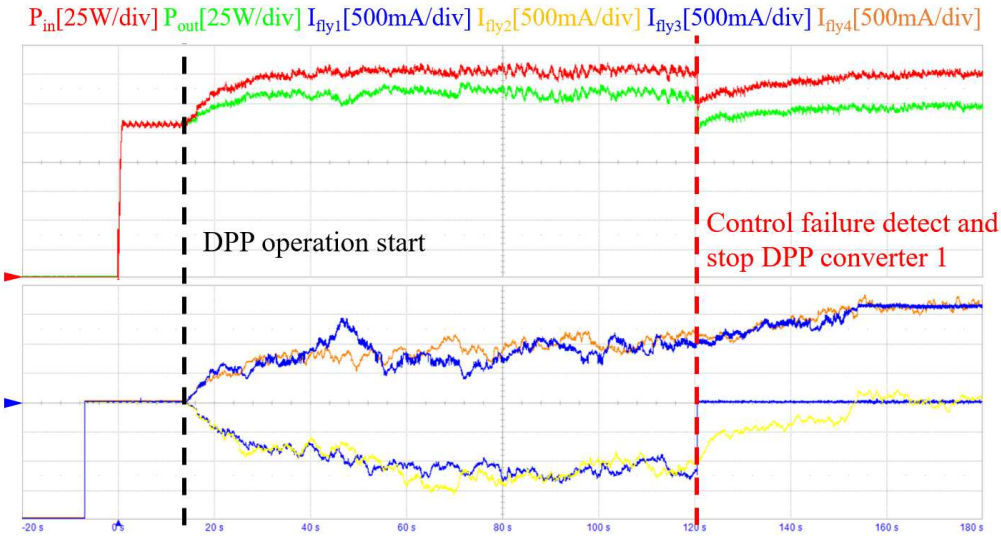

(e) DPP converter secondary open fault condition

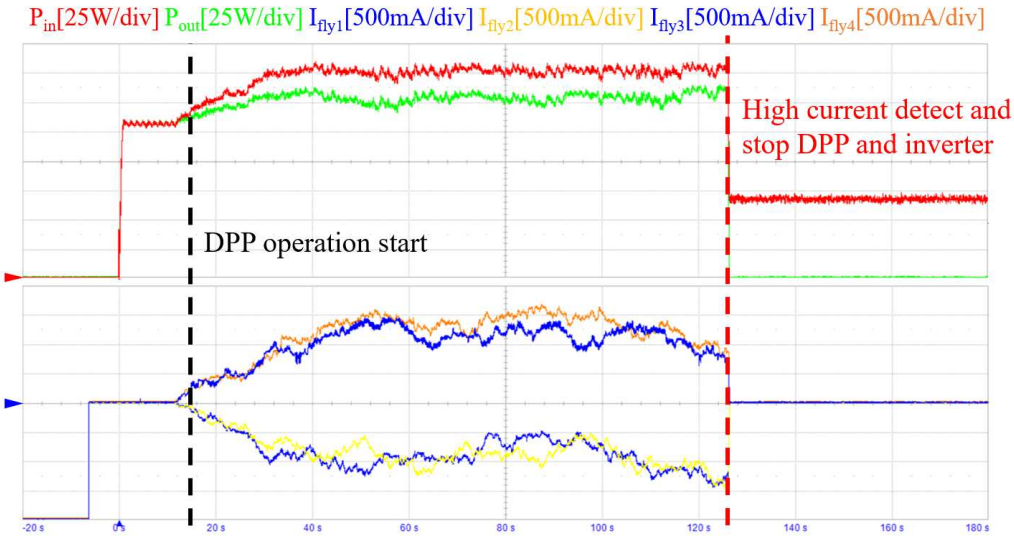

(f) DPP converter secondary short fault condition

Fig. 5.15. PHIL simulation result for DPP protection algorithm by fault condition.

ULSAN NATIONAL INSTITUTE OF SCIENCE AND TECHNOLOGY

VI. Further Works: DPP for Multiple String Diode PV Modules

The typical PV series connection system consists of parallel diodes for each PV string. In general, a DPP system operates by configuring one DPP converter per PV string.as shown in Fig. 6.1(a) [30]. Under the conditions of Fig. 6.1 (a), a series-connected system can produce 150 power in all three panels, yielding a total of 450 power, or giving up the power of shaded panels and 600 in the other two panels. The DPP system is capable of generating 150 shaded panels and 300 remaining panels all with 750 power. As a result, the DPP system achieves higher generation power than the series connection system under the corresponding shading conditions. However, a typical PV module forms several strings by connecting several internal diodes to one panel in order to generate power more advantageously in various shade conditions. The DPP system connecting the DPP converter to these PV modules is shown in Fig. 6.1(b). Under these shading conditions, the series-connected system can produce 150 power for all three panels, yielding a total of 450 power, or giving up one string of shaded panels and 800 power. This is higher than the 750 power of the DPP system. Thus, shadowing conditions are confirmed in

TABLE XIII ARITHMETIC CALCULATION POWER GENERATION BY PV SYSTEM

	One string in panel, one converter per panel	Three string in panel, one converter per panel	Three string in panel, three converter per panel
	Produced Output MPP Power in corresponding shading condition		
Series system	450 or 600	450 or 800	450 or 800
DPP system	750	750	850

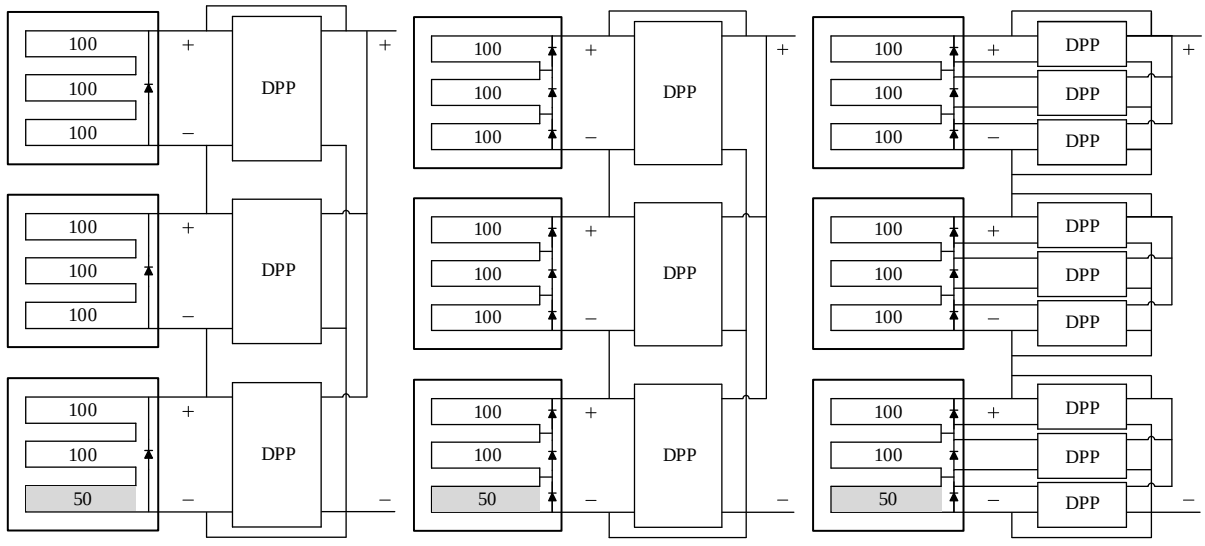

(a) One converter per one string (b) One converter per three string (c) Three converter per three string

Fig. 6.1. DPP system structure according to internal diode structure

ULSAN NATIONAL INSTITUTE OF
SCIENCE AND TECHNOLOGY

which the DPP system generates lower power than a serial connection. This problem can be solved by configuring the DPP converter for each string. This problem can be solved with the system shown in Fig. 6.1(c), which consists of a DPP converter for each string. In this system, the DPP system's generated power is 850, the maximum power of each string, which is higher than the generated power of a series-connected system. However, this increases the number of DPP converters, which is disadvantageous compared to configuring a DPP converter per panel in an actual system implementation.

This chapter presents the DPP operation on/off algorithm in the DPP system where multiple strings exist in the PV module. This does not increase the number of DPP converters but performs the DPP operation in the shading condition where the DPP system is advantageous and the series connected-system operation in the shading condition where the series-connected system is advantageous. The algorithm is verified by simulation results.

6.1 DPP On/Off Algorithm for Multiple String PV Modules

In the DPP system of a multiple string PV module, there is a partial shading condition in which the generation amount of the series-connected system is higher than that of DPP system. Therefore, in this chapter, this thesis propose an on/off algorithm that can select higher generation power according to the shadowing condition by turning on/off DPP operation while checking the generation amount of PV system. Additional PV module diode operation also provides conditions for generating more power than conventional DPP systems. In addition, the amount of insolation of all PV modules can reduce unnecessary losses by turning off the DPP operation even in the same condition.

The confirmation of generated power is performed in two methods. First of all, the DPP operation is periodically turned on/off to compare the power before and after to determine the operation of higher power. It can determine the DPP operation on/off even in the case where the change in the solar irradiance changes slowly. However, if the on/off change period is set too short, the total generated power is lowered, so it is necessary to set the appropriate period.

Another method is to turn on/off the DPP operation when the output power changes abruptly within a short time and determine the higher power after comparing the power before and after. This can determine the DPP operation on/off in a situation where the solar irradiance changes drastically.

Fig. 6.2 shows the DPP on/off algorithm flow for multiple string PV modules. For each periodic time step and power change event, it determines whether to operate through DPP operation on/off. The variables of periodic time step and power change event in the figure are values that have not been optimized. This will be optimized through actual experiments, and after the optimization, the effectiveness of the proposed algorithm will be even greater. Because the on/off algorithm requires measuring the power of the DPP system, the sensor configuration in Fig. 2.5 (b) should be used. Because the on/off algorithm requires measuring the power of the DPP system, the sensor configuration in Fig.

ULSAN NATIONAL INSTITUTE OF SCIENCE AND TECHNOLOGY

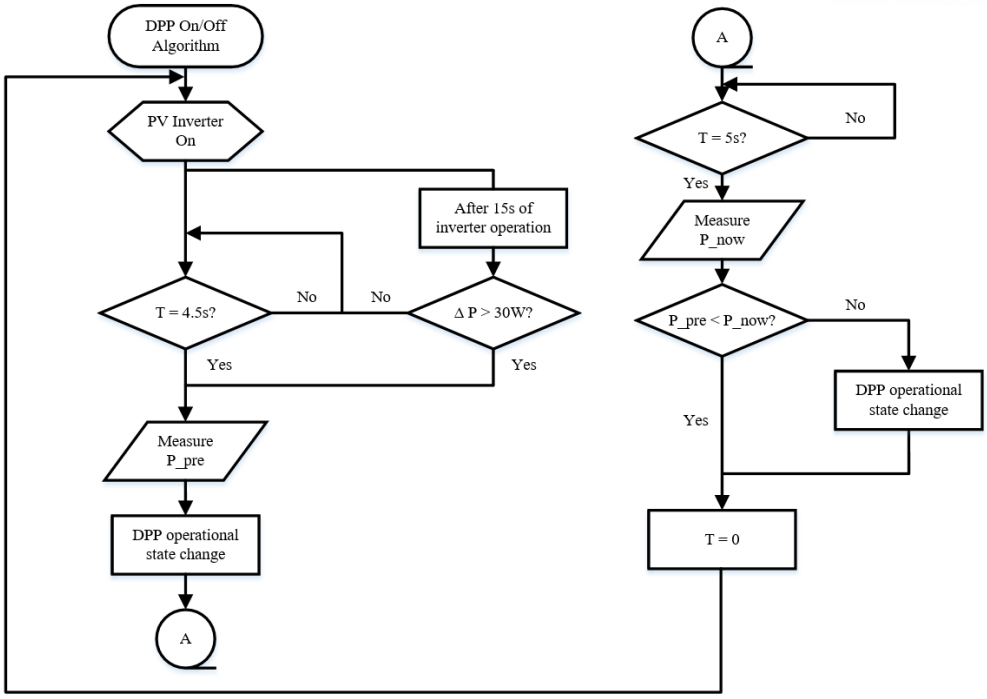

Fig. 6.2. DPP on/off algorithm flow for multiple string PV modules

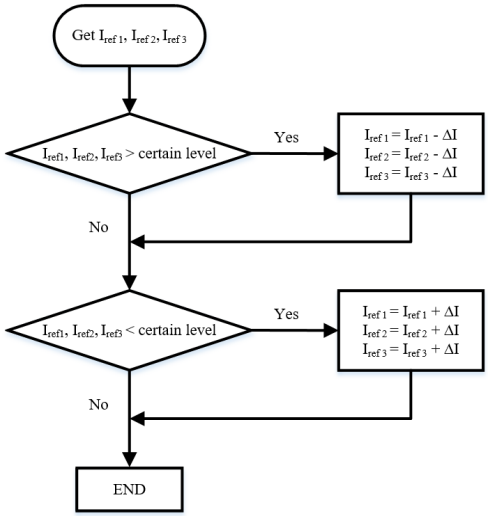

Fig. 6.3. Additional algorithm for power maximize DPP algorithm without voltage balancing

2.5 (b) should be used. However, while maximizing the voltage of each PV module can maximize the input power, it does not limit the converter operating conditions, resulting in large converter power change losses. Therefore, an additional algorithm is constructed to limit the sum of the DPP converter current commands in Fig. 6.3 to the power maximization DPP algorithm. Thus, the DPP system is constructed that maximizes the power of the PV modules and limits the operation of unnecessary converters. The proposed on/off algorithm is applied to this system to compare the simulation results with the conventional voltage maximize DPP system.

ULSAN NATIONAL INSTITUTE OF
SCIENCE AND TECHNOLOGY

6.2 Simulation Results

In this chapter, the DPP system on/off algorithm is verified by simulation. Fig. 6.4 shows the simulation configuration. The DPP system is composed of three PV modules, and the model that needs shading by strings inside the PV module is composed of individual PV strings inside. Fig. 6.5 shows the P-V curve simulation results of the conventional series-connected system and DPP system by partial shading conditions. The MPP power of the *P-V* curve is listed in Table XIIII. In Case 1, where one panel is all shaded, the DPP system generates more power than the series-connected system. However, in Case 2 and Case 3, where only one of the panel strings is shaded, the series-connected system generates more power than the DPP system. In this case, more power can be obtained by turning off the DPP operation and operating in a series-connected system.

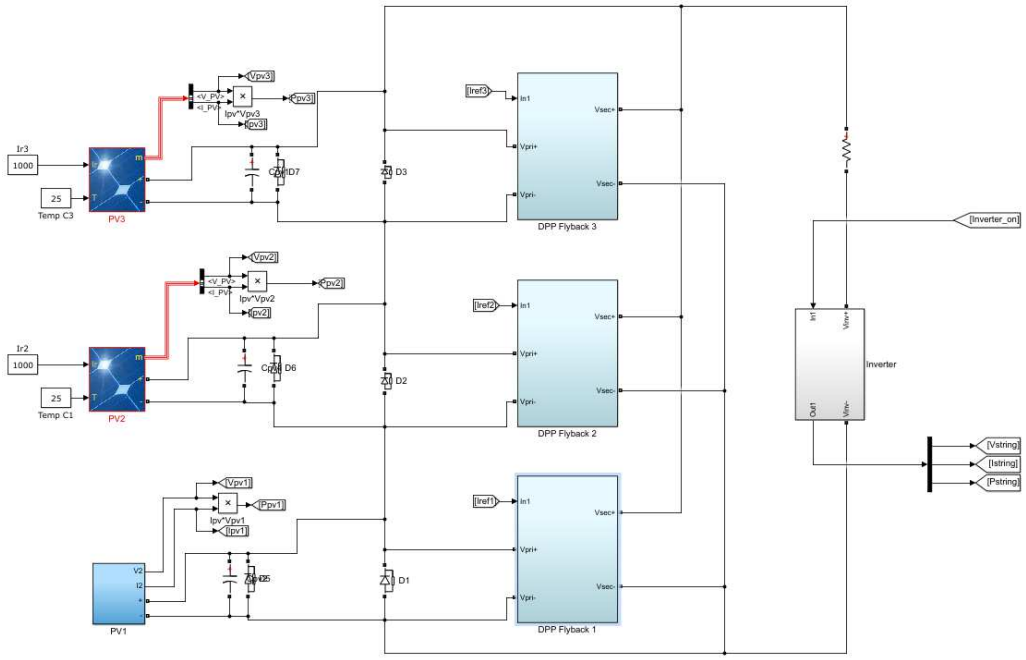

(a) Overall simulation schematic

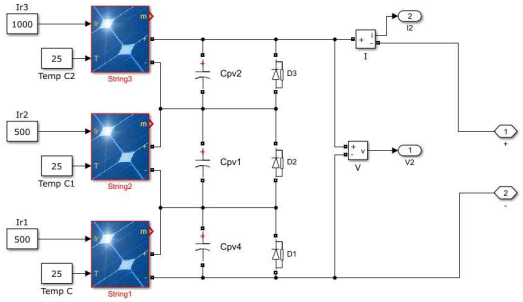

(b) Multiple string PV module

Fig. 6.4. Simulation configuration of the DPP on/off algorithm for multiple string PV modules

ULSAN NATIONAL INSTITUTE OF SCIENCE AND TECHNOLOGY

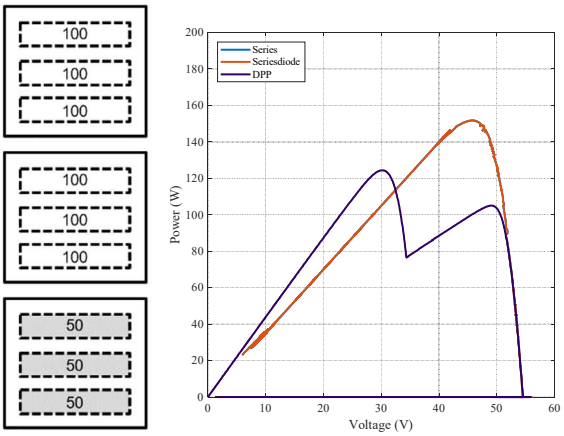

(a) Case 1

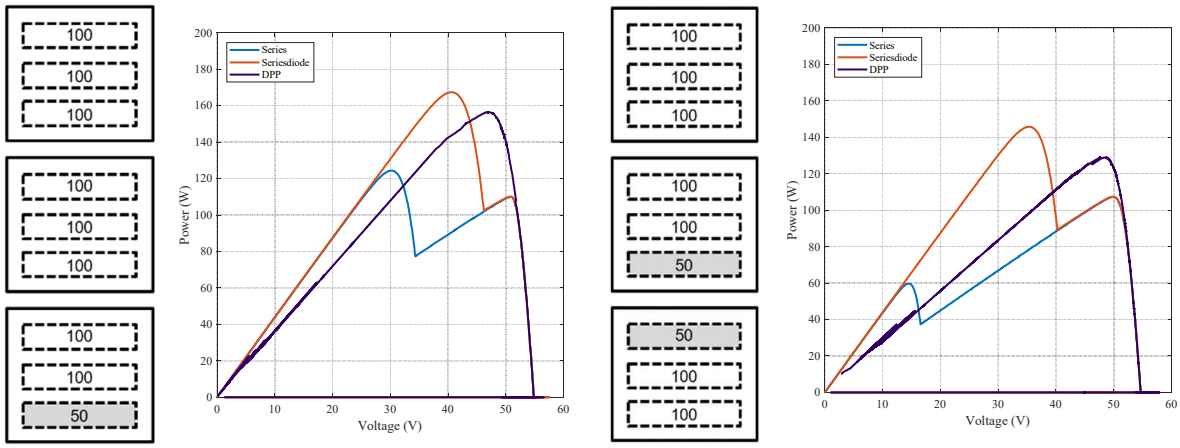

(b) Case 2 (c) Case 3

Fig. 6.5. *P-V* characteristic comparison of series system with internal diode and DPP system

TABLE XIIII THE MPP POWER OF P-V CHARACTERISTIC CURVE

	MPP Power		
	Series	Series diode	DPP
Case 1	124.4 W	124.4 W	151.7 W
Case 2	124.4 W	167.4 W	156.6 W
Case 3	107.3 W	145.7 W	129.1 W

6.2.1 Periodic Time Step

Fig. 6.6 shows the On / Off algorithm periodic time step simulation results. The simulation waveform on the left is the result of the conventional DPP system, and the simulation waveform on the right is the result of the DPP system with the proposed on/off algorithm. In the conventional DPP system, the DPP operation is always performed, while the proposed system determines whether the operation is

ULSAN NATIONAL INSTITUTE OF
SCIENCE AND TECHNOLOGY

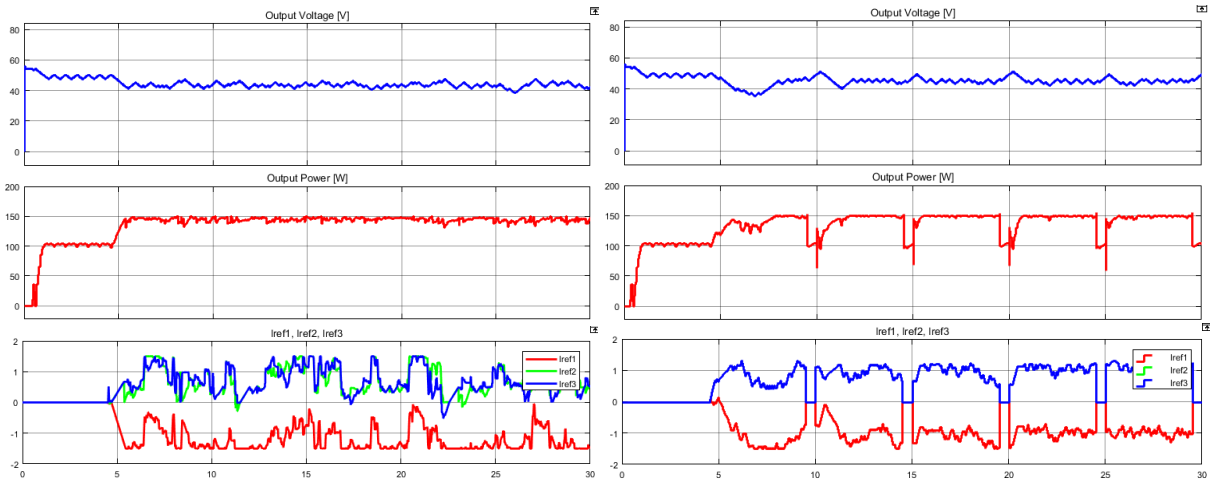

(a) Case 1

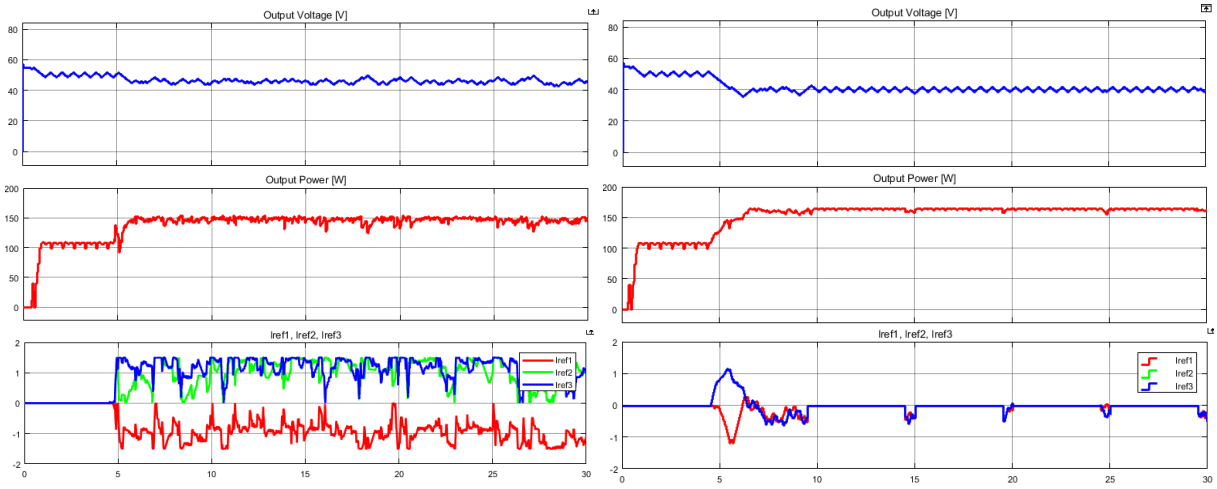

(b) Case 2

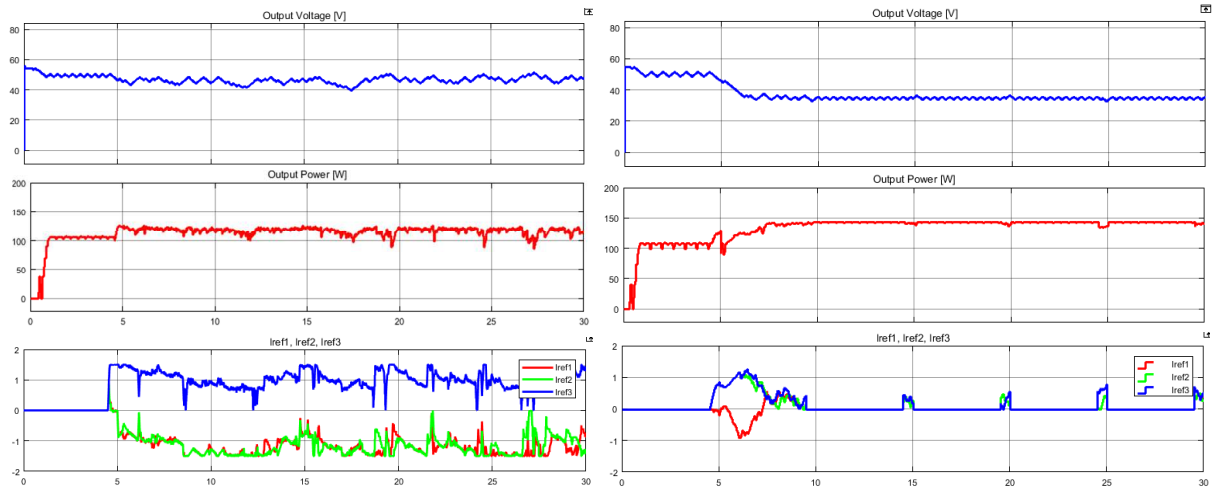

(b) Case 3

Fig. 6.6. On/Off algorithm periodic time step simulation results

ULSAN NATIONAL INSTITUTE OF SCIENCE AND TECHNOLOGY

TABLE XV AVERAGE POWER COMPARISON OF ON/OFF ALGORITHM

	10 ~ 30s Average Power	
	Conventional DPP System	On/Off Algorithm DPP System
Case 1	145.1 W	142.1 W
Case 2	147.3 W	164.5 W
Case 3	116.7 W	143.2 W

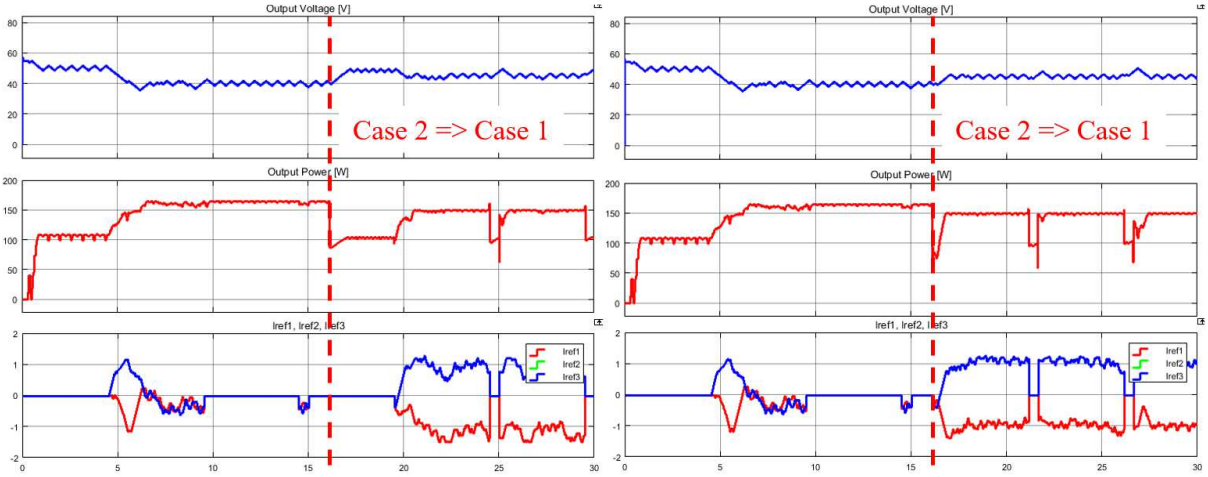

Fig. 6.7. Simulation result of the power change event

performed through the DPP operation on/off. Table XV shows average power comparison of on/off algorithm during steady state operation of the system. In case 1, where the amount of power generated by the DPP system is higher, the power generated by the conventional DPP system without operation discrimination is greater. However, since the power generation difference is not large and simulation takes a long time, the determination cycle is set to a short time of 5 seconds, so the difference will be further reduced if a more suitable period is set in the actual experiment. In case 1 and case 2 where the generation amount of the serial connection system is larger, since the DPP operation is turned off after the DPP operation is determined, it can be seen that the generation power of the DPP system using the proposed on/off algorithm is larger.

6.2.2 Power Change Event

Fig. 6.7 shows the simulation result of the power change event. In the simulation waveform on the left, the on/off determination process is not performed immediately at the large power change. However, in the simulation waveform on the right, higher generation power can be obtained by on/off discrimination at the time of large power change. Using these power change events, it is possible to respond to an immediate change in solar radiation. As a result, the effectiveness of the proposed DPP operation on/off algorithm is verified through simulation results.

ULSAN NATIONAL INSTITUTE OF
SCIENCE AND TECHNOLOGY

VII. Conclusion

In this thesis, DPP system for PV power generation system is described. An algorithm method that combines voltage balancing and total voltage maximization to reduce the number of current sensors is presented and experimentally verified. Design methodology of bidirectional flyback converter for PV-to-bus DPP structure is also described. Through this methodology, flyback converters with optimized DCM operation that is not affected by the reverse recovery characteristics of the output side switch antiparallel diode are designed. This thesis develops a protection algorithm to improve the reliability of the DPP system and verify the protection algorithm. For this purpose, a real-time DPP system model with high accuracy and adequate calculation time, and the situation of short circuit, open fault and flyback converter primary and secondary short circuit and open fault of PV module were modeled. Besides, as an indoor experimental method to confirm the developed DPP system performance, the PV emulation method which compensates the accuracy in MPP. The experimental results confirmed output power of the series connection and the DPP system under various partial shade conditions. As further work, an on/off algorithm suitable for DPP for several string diode PV modules is proposed and verified by simulation. Later, on/off algorithm suitable for DPP for several string diode PV modules will be experimentally verified.

ULSAN NATIONAL INSTITUTE OF
SCIENCE AND TECHNOLOGY

REFERENCES

1. T. Esram, P. T. Krein, B. T. Kuhn, R. S. Balog, and P. L. Chapman, “Power electronics needs for achieving grid-parity solar energy costs,” in *Proc. IEEE Energy 2030 Conf.*, Nov. 2008.

2. J. Bai, Y. Cao, Y. Hao, Z. Zhang, S. Liu, F. Cao, “Characteristic output of PV systems under partial shading or mismatch conditions,” *Solar Energy,* Vol. 112, pp. 41-54, Sep. 2014.

3. K. A. Kim and P. T. Krein, “Reexamination of Photovoltaic Hot Spotting to Show Inadequacy of the Bypass Diode,” *IEEE Journal of Photovoltaics*, vol. 5, no. 5, pp. 1435-1441, Sep 2015.

4. C. Olalla, C. Deline, D. Clement, Y. Levron, M. Rodriguez and D. Maksimovic, "Performance of Power-Limited Differential Power Processing Architectures in Mismatched PV Systems," in *IEEE Transactions on Power Electronics,* vol. 30, no. 2, pp. 618-631, Feb. 2015.

5. S. Chen, T. Liang and K. Hu, "Design, Analysis, and Implementation of Solar Power Optimizer for DC Distribution System," *IEEE Transactions on Power Electronics,* vol. 28, no. 4, pp. 1764-1772, April 2013.

6. Q. Li and P. Wolfs, "A Review of the Single Phase Photovoltaic Module Integrated Converter Topologies with Three Different DC Link Configurations," *IEEE Transactions on Power Electronics,* vol. 23, no. 3, pp. 1320-1333, May 2008.

7. C. Liao, W. Lin, Y. Chen and C. Chou, "A PV Micro-inverter With PV Current Decoupling Strategy," *in IEEE Transactions on Power Electronics,* vol. 32, no. 8, pp. 6544-6557, Aug. 2017.

8. K. A. Kim, P. S. Shenoy and P. T. Krein, “Converter Rating Analysis for Photovoltaic Differential Power Processing Systems,” *IEEE Transactions on Power Electronics,* Vol. 30, No. 4, pp. 1987-1997, April 2015.

9. Y. Levron, D. R. Clement, B. Choi, C. Olalla, D. Maksimovic, “Control of submodule integrated converters in the isolated-port differential power-processing photovoltaic architecture,” *IEEE Journal of Emerging and Selected Topics in Power Electronics,* Vol. 2, No. 4, pp. 821-832, Dec. 2014.

10. G. Chu, H. Wen, L. Jiang, Y. Hu, X. Li, “Bidirectional flyback based isolated-port submodule differential power processing optimizer for photovoltaic applications,” *Solar Energy,* Vol. 158, pp. 929-940, Oct. 2017.

11. Y. Jeon and J. Park, "Unit-Minimum Least Power Point Tracking for the Optimization of Photovoltaic Differential Power Processing Systems," *IEEE Transactions on Power Electronics,* vol. 34, no. 1, pp. 311-324, Jan. 2019.

12. Y. Jeon, K. Kim, J. Park. “Differential Power Processing System for the Capacitor Voltage Balancing of Cost-effective Photovoltaic Multi-Level Inverters.” *Journal of Power Electronics,* Vol. 17 No. 4, pp. 1037-1047, Jul 2017.

ULSAN NATIONAL INSTITUTE OF SCIENCE AND TECHNOLOGY

13. F. Wang, T. Zhu, F. Zhuo and H. Yi, "An Improved Submodule Differential Power Processing-Based PV System with Flexible Multi-MPPT Control," *IEEE Journal of Emerging and Selected Topics in Power Electronics*, vol. 6, no. 1, pp. 94-102, March 2018.

14. P. S. Shenoy, K. A. Kim, B. B. Johnson, P. T. Krein, "Differential power processing for increased energy production and reliability of photovoltaic systems," *IEEE Trans. on Power Electronics*, Vol. 28, No. 6, pp. 2968-2979, Jun. 2013.

15. C. Olalla, D. Clement, M. Rodriguez, and D. Maksimovic, "Architectures and control of submodule integrated dc-dc converters for photovoltaic applications," *IEEE Trans. Power Electron.*, vol. 28, no. 6, pp. 2980–2997, Jun. 2013.

16. X. H. Mai, S. Kwak, J. Jung and K. A. Kim, "Comprehensive Electric-Thermal Photovoltaic Modeling for Power-Hardware-in-the-Loop Simulation (PHILS) Applications," in *IEEE Transactions on Industrial Electronics*, vol. 64, no. 8, pp. 6255-6264, Aug. 2017

17. N. Femia, G. Lisi, G. Petrone, G. Spagnuolo, and M. Vitelli, "Distributed maximum power point tracking of photovoltaic arrays: Novel approach and system analysis," *IEEE Trans. Ind. Electron.*, vol. 55, no. 7, pp. 2610–2621, Jul. 2008.

18. R. Bell and R. C. N. Pilawa-Podgurski, "Decoupled and distributed maximum power point tracking of series-connected photovoltaic submodules using differential power processing," *IEEE J. Emerg. Sel. Topics Power Electron.*, vol. 3, no. 4, pp. 881–891, Dec. 2015.

19. R. Pilawa-Podgurski and D. Perreault, "Submodule integrated distributed maximum power point tracking for solar photovoltaic applications," *IEEE Transactions on Power Electronics*, vol. 28, pp. 2957 –2967, Jun. 2013.

20. H. Jung, "Segmented Differential Power Processing Structure for Large-Scale Photovoltaic Systems," *Department of Electrical Engineering, Graduate School of UNIST,* 2019.

21. R. Siemieniec, O. Blank, M. Hutzler, L. J. Yip and J. Sanchez, "Robustness of MOSFET devices under hard commutation ofthe body diode," *2013 15th European Conference on Power Electronics and Applications (EPE)*, Lille, pp. 1-10, 2013.

22. H. Kim and J. Park, "Isolated bidirectional switched-capacitor flyback converter," *2014 International Power Electronics and Application Conference and Exposition, Shanghai,* pp. 279-284, 2014.

23. S. Park, M. Kim, H. Jeong, T. Kim, K. A. Kim, and J, Jung, "Bidirectional Flyback Converter Design Methodology for Differential Power Processing Modules in PV Applications," *The Transactions of The Korean Institute of Power Electronics*, 24(5), 379-387, 10, 2019.

24. K. Venkatachalam, C. Sullivan, T. Abdallah, and H. Tacca, "Accurate prediction of ferrite core loss with nonsinusoidal waveforms using only Steinmetz parameters," *in Proc. IEEE Workshop on Computers in Power Electronics*, pp. 36-41, June 2002.

25. S. Qin, K. A. Kim and R. C. N. Pilawa-Podgurski, "Laboratory emulation of a photovoltaic module for controllable insolation and realistic dynamic performance," *2013 IEEE Power*

ULSAN NATIONAL INSTITUTE OF SCIENCE AND TECHNOLOGY

and Energy Conference at Illinois (PECI), Champaign, IL, pp. 23-29, 2013.

26. R. Ayop and C. W. Tan, “Rapid Prototyping of Photovoltaic Emulator Using Buck Converter Based on Fast Convergence Resistance Feedback Method,” *IEEE Transactions on Power Electronics*, vol. 34, no. 9, pp. 8715-8723, Sep. 2019.

27. Opal-rt, “Concept of the PHIL simulation” [Online]. Available: https://www.opal-rt.com/

28. X. H. Mai, S. Kwak, J. Jung and K. A. Kim, "Comprehensive Electric-Thermal Photovoltaic Modeling for Power-Hardware-in-the-Loop Simulation (PHILS) Applications," *in IEEE Transactions on Industrial Electronics*, vol. 64, no. 8, pp. 6255-6264, Aug. 2017

29. S. Amini Akbarabadi, M. Sucu, H. Atighechi and J. Jatskevich, "Numerical average value modeling of second order flyback converter in both operational modes," *2013 IEEE 14th Workshop on Control and Modeling for Power Electronics (COMPEL)*, Salt Lake City, UT, 2013, pp. 1-6.

30. H. Jeong, H. Lee, Y. Liu and K. A. Kim, "Review of Differential Power Processing Converter Techniques for Photovoltaic Applications," *in IEEE Transactions on Energy Conversion*, vol. 34, no. 1, pp. 351-360, March 2019.